

Response to Anne Jefferson

Manuscript Number: ACP-2015-670

Manuscript Title: Aerosol optical properties in the southeastern United States in summer – Part 1: Hygroscopic growth

The authors thank Dr. Jefferson for the comment on application of the gamma parameterization. Below is the comment, followed by our response.

The power law gamma approximation of the extinction hygroscopic growth assumes a metastable aerosol in an RH regime of continuous growth. The fit falls apart at low RH values where $f(RH)$ values are essentially 1.0 over an extended RH range, i.e. the curve flattens out. For aerosol with a high inorganic composition you run the risk of the aerosol efflorescing below 30% RH. Try anchoring the fit at the lower RH value around 30-40% and the gamma fit will work much better. Assume that extinction growth is negligible from the low RH value of 11% to ~40% RH. Adjust the lower RH value in your fit to 30-40%. The fit will work much better. In future measurements set the RH in the low RH extinction cell to ~30-40%.

This comment is correct for an aerosol that displays phase change behavior, as is common for many remote background and marine aerosols. We now include a plot of the gamma parameterization using $RH_0=35\%$ (Fig. 7a), which indeed produces a better fit to the medium and high RH values (and assumes no aerosol water at $RH<35\%$). But this approach is unphysical for a constantly deliquescing aerosol, which we believe is the case for the organic-dominated aerosol in the southeastern US. Additional data presented in the Appendix and Supplemental Materials (for different environments than we measured here) also show a more continuous deliquescence curve for the majority of polluted, presumably organic-dominated cases. And lacking additional information, what value of RH_0 should we choose? This essentially makes the gamma parameterization a two-parameter fit, with gamma and RH_0 as the fitted variables. For our three-point $f(RH)$ measurements we prefer to use a physically based, single-parameter fit (the κ_{ext} parameterization) that approaches physically reasonable values at the lower limit of atmospheric RH conditions, and that better simulates $f(RH)$ for $RH > 90\%$, as shown in the Appendix and Supplemental Materials.

Response to Reviewer 1

Manuscript Number: ACP-2015-670

Manuscript Title: Aerosol optical properties in the southeastern United States in summer – Part 1: Hygroscopic growth

The discussion below includes the complete text from the reviewer, along with our responses and corresponding changes made to the revised manuscript in bold. The authors thank the reviewer for useful comments that have improved the manuscript.

We note that the manuscript has been substantially reorganized in response to Reviewer 2. All line and page numbers below refer to the original manuscript.

Scientific significance:

Good – Hygroscopicity of aerosol is still highly uncertain, despite being an important factor in determining aerosol direct radiative forcing. The data on OA K_{chem} are therefore of high scientific importance, especially since they fall on the low end of the expected range and are supported by a robust analysis. The new fit parameter to describe hygroscopic growth, K_{ext} , is a moderate improvement over the most commonly used fit parameter, γ , and is of sufficient value to merit publication.

Scientific quality:

Excellent – This paper combines careful measurements, quantification of uncertainties where this is possible and acknowledgement where it is not, and a robust, comprehensive and clear analysis.

Presentation quality:

Excellent – The paper is very well-written and organized. The analysis presented supports the conclusions. I wish all papers I reviewed were this well-written. This paper should be accepted for publication once the following minor points are addressed:

1. The Abstract and Conclusions state that the new K_{ext} parameter formulation does a better job of describing the observed aerosol hygroscopic growth than does the traditionally-used γ fit parameter/formulation. This is true, but the improvement over the γ fit is only, on average, 20% for the RH (70%) where the bias in the γ fit is greatest; at other RHs the γ fit is better. By not quantifying the improvement in the Abstract/Conclusions, the reader gets the sense that improvement by using the new K_{ext} over the γ fit is perhaps greater than it is. Please quantify the improvement in the Abstract and Conclusions.

The manuscript has been modified to focus on the observed hygroscopicity rather than the new parameterization. We note that there are much larger potential differences in the two parameterizations for RH > 90%, and show evidence in the Appendix and Supplemental Materials that the κ_{ext} parameterization does a better job describing hygroscopicity over the full range of RH values.

2. As noted in the comment by Anne Jefferson, the goodness of the γ fit/formulation will depend in part on what is used for RH_o in Eqn. 1, and this should at a minimum be acknowledged in the paper.

We include a plot of the γ parameterization using $RH_o=35$ (Fig. 7a), which indeed produces a better fit to the medium and high RH values. But this approach is unphysical for a constantly deliquescent aerosol, which we believe is the case for the organic-dominated composition in the southeastern U.S. Additional data presented in the Appendix and Supplemental Materials (for different environments than we measured here) also show a more continuous deliquescence curve for the majority of cases. And lacking additional information, what value of RH_o should we choose? This essentially makes the γ parameterization a two-parameter fit, with γ and RH_o as the fitted variables. We strongly prefer to use a physically based parameterization that approaches reasonable values at the lower limit of atmospheric RH conditions, and that better simulates $f(RH)$ for RH >90% as shown in the Appendix and Supplemental Materials.

3. pg 25705 lines 5-12: "The parameter K_{chem} may be calculated from the volume weighted contribution due to species i , K_i , which are determined: : ." Please be explicit here: contribution to what? contribution to hygroscopicity? to mass?

This sentence is rephrased to: "The value of κ_{chem} for the mixed particle composition may be calculated from the volume weighted average of the κ_{chem} of each species i , κ_i , that contributes to the aerosol composition."

4. pg 25707, line 21: Sub-micron sea salt was assumed to be zero. Is there any evidence to support that sub-micron sea salt was negligible? Given its high $f(RH)$, even a small mass contribution might significantly affect extinction at higher RH.

We did not measure refractory aerosol composition on the aircraft. Contemporaneous measurements (Guo et al., 2015) at the SOAS surface site in Centreville, Alabama (near which we flew several profiles and low passes for purposes of comparison), show a negligible fine mode contribution from sea-salt. This is now stated in section 2.3.

5. pg 25709, lines 24-27 & Figure 2 & Figure 4: Figures 2 and 4 only show/include data (and regression) for a section of one flight.

a) Why only fit data from 11:10-11:45 from that flight?

b) What is the fit/regression for the full data set?

c) How is the comparison of the K_{ext} and gamma fit affected by inclusion of more of the field data?

d) Fig. 2b. There seems to be two groups of data: $<50 \text{ Mm}^{-1}$ there is excellent agreement; $>50 \text{ Mm}^{-1}$ the calculated extinction is higher than the measured extinction. This is clearly the case for another high-extinction period 12:10-12:20 shown in Fig. 2a, but not included in Fig. 2b. Again, this makes me question why only data from 11:10-11:45 are include in the comparison, as well as whether the fit is not as robust at high extinction.

The data originally presented in Figs 2 and 4a were not from the data included in the analysis, but were presented as an example from another flight in SENEX because extinction values were nearly constant as the plane flew at a level altitude, allowing us to average over 35 minutes and get good statistics. In place of this example, we now provide as an example a profile (Fig. 3c) that was included in the data selected for the analysis. The $f(RH)$ curve from this profile is in Fig. 7, which also includes histograms of $f(RH)$ for all the analyzed data. Further, we provide a composite profile (Fig. 4b) produced from all of the selected profiles that shows median and variability data for extinction and $f(RH)$ and how well the fits to the κ_{ext} and gamma parameterization represent $f(RH)$ at $\sim 70\%$ RH. The better performance of the κ_{ext} parameterization for most of the data is shown by the histograms in Fig. 7c. The histograms differ slightly from the previous manuscript because we are now including all data when the high RH channel was at 85% RH or higher (before we were filtering at 88% RH).

e) (small point: "over the time period from 11:10 and 11:45 LT" should be reworded to, e.g. "over the time period 11:10-11:45 LT")

This is no longer relevant as this data example has been removed.

6. pg 25711, lines 26-27: "This $\sim 20\%$ effect on $f(RH)$ due to refractive index change for $RH \sim 90\%$ (Hegg et al., 1993) can be ignored to first order." Here it is asserted that a 20% effect "can be ignored to first order" – yet the average 20% bias caused by using the gamma fit was earlier presented as a significant enough error to be worth exploring an entirely different fit formulation. This seems to be an inconsistency.

This is why the κ_{ext} formulation does not exactly predict the change in extinction with humidity-- it's only an approximation that must be used parametrically (fitted to data) rather than as an exact prediction from first principles. This issue is now discussed in Appendix section A.1., where we state, "The volume-extinction approximate proportionality in Eq. (A1) applies for an aerosol of

constant refractive index, which is not the case for an atmospheric aerosol particle growing by addition of water with increasing RH (Hänel, 1976; Hegg et al., 1993). The methodology to calculate ambient extinction (Section 2.3), which incorporates the aerosol composition and size distribution measurements, can be used to estimate the effect of aerosol water on the refractive index and its impact on extinction. Using this approach, the calculated mean decrease in refractive index caused by condensed water reduces extinction by a factor of 0.81 +/- .03 for the ~70% RH channel and by 0.71 +/- .03 for the ~90% RH channel. Because of this effect and the rough proportionality between particle volume and extinction, Eq. A1 [the κ_{ext} parameterization] is an approximation that may be used only parametrically to interpolate and extrapolate from discrete measurements on the $f(\text{RH})$ curve. However, it is a physically based representation of the expected functional form of $f(\text{RH})$, unlike alternative parameterizations."

7. pg 25715, line 20: I think there is a typo (misplaced "r"?) toward the end of the line: " $K_{\text{chem}}r$ ".

Corrected.

Finally, we have reprocessed all of the extinction values calculated from the AMS and size distribution measurements using the best estimate of κ_{chem} for OA of 0.05 from our measurements, rather than the 0.076 from the literature we used previously. This improves theoretical and measured comparison of $f(\text{RH})$ at the high humidity condition (Fig. 5).

Response to Reviewer 2

Manuscript Number: ACP-2015-670

Manuscript Title: Aerosol optical properties in the southeastern United States in summer – Part 1: Hygroscopic growth

The discussion below includes the complete text from the reviewer, along with our responses and corresponding changes made to the revised manuscript in bold. The authors thank the reviewer for useful comments that have improved the manuscript.

Brock et al. use airborne profiles of aerosol properties performed in the southeastern United States to investigate the hygroscopic effect of aerosol particles on their extinction coefficient at three distinct relative humidities (RH). A new parametrisation is presented that is found to more adequately describe the observations than a different single parameter equation (γ -equation).

Although I have no doubts as to the high quality and scientific significance of the presented data, I see some major shortcomings in the analysis and the following interpretation. First of all, the paper uses airborne profiles of measured optical extinction enhancement factors (plus size distribution and composition measurements) but no profiles or interpretation of these are shown (in contrast to the title of the presented manuscript). This could be due to the fact that these will be shown in a companion paper. However, it is not acceptable that the data selection criteria that lead to the presented results are not accessible for the review process (quote from page 25699, line 20: "Part 2 also contains details of the selection of data for the analysis of both papers ...").

Secondly, the proposed parametrization is based on measurements at one dry and two elevated relative humidities only, which is an understandable and necessary compromise for airborne measurements. However, I doubt that three values are sufficient to propose a new and improved parametrization bearing in mind that many aerosol types show hysteresis effects which can not be described by a simple γ -fit. Due to the limited number of elevated RH measurements it is important that the authors present and discuss the (hygroscopic) calibration of their instrument with nebulized salts prior to each campaign or flight.

The paper would be substantially improved by

(a) more focused discussion of the actual profile measurements of the extinction enhancement, its vertical and spatial variation, its link to chemical composition and air mass origin (as the manuscript title also implies); and

(b) less focus on the parametrization of a three point measurement. There are further detailed comments given below (in arbitrary order) that should be adequately addressed before this manuscript can be published in ACP. It is for these reasons that I recommend major revisions.

In response to these comments, we have made substantial changes to the content and structure of the manuscript, as requested. The outline of the original manuscript was:

1. Introduction

2. Methods

2.1 Aircraft instrumentation

2.2 Corrections to UHSAS size distributions for refractive index

2.3 Method to calculate ambient extinction

2.4 Uncertainty in calculated and measured extinction

3. Results and analysis

3.1 Parameterizing $f(\text{RH})$

3.2. Relationship between κ_{chem} and κ_{ext}

3.3 Constraints on the hygroscopicity of OA

3.4 Comparison of airborne and ground-based data

4. Conclusions

The revised manuscript diverges in structure from the original beginning in Sect. 3:

3. Results and analysis

3.1 Selection of data

3.2 Observed aerosol composition and hygroscopicity

3.3 Constraints on the hygroscopicity of OA

3.4 Parameterizing $f(RH)$

3.5 Comparison of airborne and ground-based data

4. Discussion and conclusions

Appendix

A.1 Derivation of the κ_{ext} parameterization

A.2 Relationship between κ_{chem} and κ_{ext}

A.3. Additional data supporting use of the κ_{ext} parameterization

Supplemental Materials

To reduce the emphasis on the parameterization of $f(RH)$, the derivation is moved to the Appendix. To provide more information on the data selection, the hygroscopicity of the aerosol, and its vertical structure, new sections 3.1 and 3.2 and two new figures have been added. These are followed immediately by a discussion of constraints on the hygroscopicity of the organic aerosol provided by our observations. Only then is the new parameterization introduced and used. In the Supplemental Materials and Appendix we provide further evidence from the literature and from additional measurements to support the use of this parameterization.

In addition to these changes we have strengthened the discussion of uncertainties in our measurements and provided more detail on the calibration of the extinction measurements.

The following new figures have been added:

Figure 2: Map of flight tracks and locations of profiles

Figure 3: Vertical profile from 2013/06/22 showing vertical structure

Figure 4: Composite vertical profile from all selected individual profiles showing median, interquartile, and interdecile values

Figure 5: $f(RH)$ at ~70% and ~90% RH calculated from the composition and size distribution measurements, and directly measured by the CRDS

Figure A4: $f(RH)$ from additional measurements in Boulder, Colorado showing hygroscopicity from 11-97% ambient RH

The original Fig. 2 has been eliminated. The original Figs. 3 and 4 have been combined in Fig. 7. The original Figs. 5, 6, and 7 have been moved to the Appendix.

- Page 25700, line 21 and page 25701, line 6: What is the exact range of measured RH inside the cells? Please give the range and standard deviation. How stable is the RH during a profile? The current values given are very vague. The dry value changes within the manuscript from <15% to <25 %. At 25% RH the influence of hygroscopic growth of organic substance can become relevant.

Section 2.1 now describes the range of values of RH in each channel: "Typically, one elevated-RH channel measured at ~70% RH (actual range 70-73%) and the other measured at ~90% RH (actual range 86-94%). Data were excluded from analysis when the RH of the high RH channel was <85%." The dry channel "measured at ~15% (actual range 8-23%)." Fig. 3 gives an example of the stability of the RH control during profiles. Histograms of the actual RH values are reported in the Supplemental Materials.

- Page 25700: As mentioned above, it should be clearly stated which profiles were selected and which criteria were applied. Showing the average profiles of $f(RH)$ and case studies would improve the quality of the paper.

The selection criteria are described more in the new Sect. 3.1, and we have added a citation to Wagner et al. (2015), who describe in great detail the selection of the profiles and the compositing technique. Figure 2 now shows a map of where the observations were made.

• Page 25701, line 10: Were the calibration measurements with ammonium sulfate conducted before each campaign or flight? Please show (at least in the reply letter) the corresponding calibration plot and state the degree of agreement in the revised manuscript. Presenting this information is critical to evaluating the usefulness of the proposed parametrization.

The CRDS has been described in detail in Langridge et al. (2011), who tested the hygroscopic response of the instrument to inorganic salts and polystyrene particles. The fact that the CRDS system is not routinely calibrated is discussed; it is a fundamental technique that is occasionally checked with an absorbing gas (ozone). More important to the measurement of $f(\text{RH})$ is the transmission efficiency of the particles, which we now describe in more detail, and the accuracy of the RH sensors and their calibration, which we also discuss now. These issues appear in the last two paragraphs of Section 2.1.

• Sect. 2.1: How were particle losses (from the inlet to the CRDS and within the CRDS) characterized and how were they treated in the data analysis?

Section 2.1 now describes the losses in the inlet and plumbing system, which are very small for the $<0.7 \mu\text{m}$ particles we analyze.

• Page 25702, line 7: The low amount of particle light extinction above 700nm is surprising to me. What was the exact range for all analysed profiles? Could this be due to losses inside the aircraft sampling lines? In the reviewers opinion, it is important to keep the influence of the coarse mode in mind since it has (even at low number concentrations) an important impact on the overall $f(\text{RH})$ (see e.g. Zieger et al, 2013, 2014).

Since our analysis is limited to measurements of particles $<0.7 \mu\text{m}$, we don't address the coarse mode aerosol. However, Brock et al. (2016; Part II) show that the coarse mode is a small fraction of the total extinction, and retrieve aerosol optical depths that are consistent with regional climatology. The coarse mode is not a major contributor to aerosol extinction in the southeastern U.S. in summertime in typical conditions.

• Sect. 2.2: How were the Mie ambiguities (or Mie wiggles) treated in the UHSAS size correction?

Because the UHSAS uses a 1053 nm laser, the Mie oscillations occur at larger sizes than considered here. The wavelength and wide scattering angles ensure a monotonic response for reasonable refractive indices (see Cai et al., 2008), although there is reduction in resolution for sizes larger than about $0.7 \mu\text{m}$ due to curve flattening.

• Sect. 2.3: The usage of k-Köhler theory to calculate optical enhancement factors and related closure studies has also been done in previous studies, which should be referenced here (see e.g. Zieger et al., 2013).

We discuss more thoroughly the literature in the introduction, and in the final section we compare our results to others, including Zieger et al. (2013). Further, we use data digitized from graphs in Zieger et al. in the Supplemental Materials to further support the use of the κ_{ext} parameterization.

• Sect. 2.4 (second last paragraph on page 25709): Please state also the relative uncertainties in $f(\text{RH})$ for the three RH channels.

The last sentence of Sect. 2.1 now reads, "Thus the uncertainty in $f(\text{RH})$ is estimated to be $\pm 11\%$ and $\pm 16\%$ for the medium and high RH channels, respectively. This uncertainty estimate does not

account for possible residual water present in particles in the ~15% RH channel, which could bias the $f(\text{RH})$ values low."

- Result section, Fig. 2: Is this a ground measurement or why is it not shown as a profile? If it is a ground based measurement, why has it been chosen? Again, it would be highly desirable if the actual profiles would be shown and discussed.

Figure 2 has been replaced with an example profile (Fig. 3).

- Fig. 2b: How does the actual $f(\text{RH})$ (calculated vs. measured) compare at the three RH's?

Figure 2 has been replaced with an example profile (Fig. 3). Figure 5 now compares calculated and measured $f(\text{RH})$ using a fixed κ_{org} of 0.05 at the medium and high RH values for all the data.

- Sect. 3.1: Defining the parametrization at $\text{RH}=0\%$ as 1 cannot be realistic for actual atmospheric conditions (due to hysteresis effects). I understand that this assumption is needed due to the limited amount of RH channels, however, a systematic error in one of the elevated RH cells could also explain why the fit is not a suitable parametrization. This is one reason why the authors have to include their instrument calibration with known hygroscopic salts and a discussion on particle losses in the revised manuscript. In addition, I find it astonishing that only a short time period (8 July 2013, 11:10-11:45) is chosen for their fit (Fig. 4a) and time series (Fig. 2a), from which it is even not clear if it is an actual airborne profile or not.

In the Supplemental Materials we show that the new parameterization does a better job than the power-law gamma parameterization for several higher resolution $f(\text{RH})$ cases from the literature. In Section A.3 we show the previously unpublished data that of $f(\text{RH})$ with continuous deliquescence behavior for a different environment. Remember also that we are measuring the deliquesced aerosol, and that it is heavily organic in composition. Of course we have never claimed that this parameterization is always better than other choices, and provide several examples of where it should not be used in Appendix A.1. We also discuss in Sect. 3.4 (last two paragraphs) the limitations on the use of this parameterization. The κ_{ext} parameterization was applied to all of the data, not just to a short time period. We found that it fit better than the gamma parameterization for more than 2/3 of our profiles, and that there are strong physical arguments for the parameterization we have developed, when applied to an organic-dominated submicron aerosol.

- Page 25711, line 26: I doubt that the change in refractive index from dry to elevated RH only has an approximate effect of 20% and thus can be ignored to first order. For example, if one takes the hygroscopic growth factor of a 200nm ammonium sulfate particle (at $\text{RH}=90\%$) to be approx. 1.7 then this will give at $\text{RH}=90\%$ a refractive index of ~1.36 (if calculated using a volume mixing ratio). The change in scattering alone will be more than 20% (at $\text{RH}=90\%$) and depending on the mode diameter up to 1 μm it will be rather a factor of 1.5 to 2.5. Please clarify and proof your assumptions e.g. by showing a further sensitivity study that accounts for changes in refractive index (e.g. by adding the extinction efficiency for $m = 1:36$ and $m = 1:33$, for pure water to Fig. 5).

Please note that we are arguing that the functional form of the κ_{ext} equation is appropriate but only approximate, not that it is a perfect predictor of the $f(\text{RH})$ curve from first principles. Also, because we are averaging across a size distribution, the effect of refractive index is reduced compared to your example, although it is not negligible. We have calculated this refractive index by comparing calculated extinction with no refractive index change to calculated extinction with a reduced refractive index from water for all of the analyzed data. As we now state in Sect. A.1, "The volume-extinction approximate proportionality in Eq. (A1) applies for an aerosol of constant refractive index, which is not the case for an atmospheric aerosol particle growing by addition of water with increasing RH (Hänel, 1976; Hegg et al., 1993). The methodology to calculate ambient extinction (Section 2.3), which incorporates the aerosol composition and size distribution measurements, can be used to estimate the effect of aerosol water on the refractive index and its impact on extinction. Using this approach, the calculated mean decrease in refractive index

caused by condensed water reduces extinction by a factor of 0.81 +/- .03 for the ~70% RH channel and by 0.71 +/- .03 for the ~90% RH channel. Because of this effect and the rough proportionality between particle volume and extinction, Eq. A1 is only an approximation that should be used parametrically to interpolate and extrapolate from discrete measurements on the f(RH) curve. However, it is a physically based representation of the expected functional form of f(RH), unlike alternative parameterizations."

- Page 25712, line 16: I suggest to delete this sentence since an argument is brought forward in terms of a measurement result that has not been published or reviewed yet and this is hard to evaluate or judge on (and I guess it is not winter 2015 since this lies in the future).

These data are now presented in the the Appendix (A.3). The previously unreported data were collected in a very different environment (winter in Colorado, with an organic and nitrate-rich aerosol) with a completely different instrument (Gordon et al., AMT, 2015). As a result we don't want to include them in the main text of this paper. But these data provide a very compelling, if limited, indication that the κ_{ext} parameterization is more broadly applicable and is appropriate even at RH >95%.

- Page 25715, line 16: It is not clear to the reviewer why the uncertainty of the organic κ should cancel out when calculating f(RH). A slight overestimation of the organic κ will also lead to an overestimation of the f(RH) (see e.g. Fig. 9a in Zieger et al, 2015) and vice versa. In general, due to the importance of the organic contribution the uncertainty of the organic κ will easily compensate other systematic errors. Please clarify.

The uncertainties that cancel are the UHSAS uncertainties and the AMS flow uncertainty, not the uncertainty in the organic fraction. The text has been clarified: "Some of the errors in the calculated extinction–UHSAS sizing bias, UHSAS counting statistics, and UHSAS and AMS flow uncertainties (Sect. 2.4)–are not independent and should cancel when calculating f(RH)."

- Page 25716 (first paragraph) and Fig. 8: Could these low organic k-values also result in the effect of a temperature dependent evaporation of inorganic component (like ammonium nitrate, see e.g. Aan de Brugh et al., 2012), which were held constant to derive the organic k?

Inorganic nitrates were insignificant in the warm summertime of the southeastern U.S. We support this assertion by referencing in Sect. 2.1 the results of Attwood et al. (2014) and Xu et al. (2015) from observations taken at the Centreville, Alabama ground site in collaboration with the airborne measurements. They report inorganic nitrate values < 0.02 $\mu\text{g m}^{-3}$.

- Table 2 is not discussed in the main text. The comparison in terms of linear regression will always be better for the extinction coefficient which is determined mainly by particle number concentration. To better evaluate the model performance to hygroscopicity measurements the authors should add a table or plot showing the comparison of the actual f(RH) modelled vs. measured. In addition, the variation in RH and the contribution of the coarse mode for each profile should be stated. Again, why were only these eight days selected?

Table 2 is referenced in the fourth paragraph of what is now Section 2.4. The new Fig. 5 now shows all the calculated vs. measured f(RH) values. The data selection is detailed in Wagner et al. (2015) and is also described better in the new Section 2.1.

- Fig. 3: What temporal averaging was applied here? In general, how was the data averaged?

Averaging of the data to 10 s is described in the new Section 2.4.

- Fig. 4b: For completeness, the ratio of calculated to measured f(RH) at RH=90% should be shown as well.

The new Fig. 5 shows this ratio.

• Fig. 7: Are the outliers determined by certain events or aerosol characteristics? Have the authors tested the different possibilities, e.g. by color-coding the points according to time, flight altitude, temperature, apparent coarse mode, mean geometric diameter? This could be a useful addition to evaluate the model performance.

This figure is now in the Appendix as Figure A.3. We have not been able to identify any systematic attribute of the outliers. Groups of outliers are associated with particular flights, but there doesn't appear to be any change in instrument performance, aerosol composition, or size distribution that would explain the groupings.

• Sect. 3.4 and Fig. 8: Please specify how the organic mass fraction was calculated (e.g. was BC included or not).

As noted in the last sentence of the old Sect. 2.2, BC was included in all calculations other than the UHSAS refractive index response correction.

Technical comments:

• Page 25703, line 3: I would remove 'of a design now commercially available' since it is not relevant for this work.

Since we do not have a publication for this DMA, by referencing the commercial instrument that is based on our prototype readers can obtain detailed specifications. We prefer to keep this comment.

• Page 25700, line 5; page 25712, line 22: Full stop missing at the end of the sentence.

Corrected.

• Page 25715, line 20: Remove the 'r' behind `_chem`.

Corrected.

• Page 25697, line 2: I would suggest to remove 'meteorological, trace gas, and' since this data is not being used in the following article.

These data are important in determining the vertical structure, as is now described in Sect. 3.1.

• Table 1: Please mention the corresponding wavelength in the caption and unit for the density.

The density units have been added. Most of the references do not provide wavelength information for the refractive index, but are invariably reported in the mid-visible.

• Fig. 6: The x-axis is a little bit confusing and at first the reader looks at 2, 3, etc. μm diameter. Better replace it by 0.2, 0.3, etc.

Graph has been modified as requested.

Finally, we have reprocessed all of the extinction values calculated from the AMS and size distribution measurements using the best estimate of κ_{chem} for OA of 0.05 from our measurements, rather than the 0.076 from the literature we used previously. This improves theoretical and measured comparison of $f(\text{RH})$ at the high humidity condition (Fig. 5) compared to the prior value.

~~approximately linear relationship between particle volume (or mass) and optical extinction (Charlson et al., 1967). The fitted parameter, κ_{ext} , is nonlinearly related to the chemically derived κ parameter used in κ Köhler theory. The values of κ_{ext} we determined from airborne measurements are consistent with independent observations at a nearby ground site.~~

~~1 Introduction~~

~~Particles in the atmosphere scatter and absorb solar radiation. Atmospheric aerosol extinction (=scattering+absorption) reduces visibility and usually cools the earth, especially over dark surfaces such as oceans and forests. Uncertainty in the direct ~~climate~~radiative forcing due to anthropogenic aerosols is the second largest contributor to total uncertainty in climate forcing (IPCC, 2013; Bond et al., 2013).~~

~~One of the most important factors affecting ambient aerosol optical extinction—hence visibility, aerosol optical depth (AOD), and direct radiative effects—is the particulate water mass, which depends on both the hydrophilic properties of the aerosol components and the relative humidity (RH). Hygroscopic water uptake changes particle size and refractive index and can lead to dramatic changes in the extinction as a function of RH due to changes in the amount of aerosol liquid water, even when dry mass is constant. ~~Since atmospheric~~Atmospheric RH is highly variable temporally, horizontally, and especially vertically, ~~so~~ aerosol water ~~plays an important role~~ ~~in~~modulates the relationship between ambient extinction and dry aerosol mass.~~

~~The relationship between atmospheric extinction and humidity has long been recognized (e.g., Wright, 1939). The coupling between particle hygroscopicity and composition and optical extinction has been evaluated experimentally and quantitatively since the work of Pilat and Charlson (1966), Covert and Charlson (1972) and Hänel (1972a; 1972b). Understanding the factors controlling the change in extinction or scattering as a function of RH, known as $f(RH)$, is important for evaluating remote sensing measurements (e.g., Brock et al., 2015; Crumeyrolle et al., 2014; Esteve et al., 2012; Ferrare et al., 1998; Hegg et al., 1993; Kotchenruther et al., 1999; van Donkelaar et al., 2015; Voss et al., 2001; Zieger et al., 2011, 2012; Ziemba et al., 2012), aerosol direct radiative forcing calculations (e.g., Attwood et al., 2014; IPCC, 2013; Kahn, 2011; Koloutsou-Vakakis et al., 1998; Nemesure et al., 1995), and atmospheric visibility estimates (e.g., Charlson et al., 1967; Malm et al., 2000). In general, particles composed primarily of organic material and dust are less hygroscopic (Duplissy et al., 2011; Petters and Kreidenweis, 2007; Zieger et al., 2015), while those that are predominantly inorganic take up water more readily (e.g., Petters and Kreidenweis, 2007; Quinn et al., 2005). Particles may exhibit sharp phase transitions as they deliquesce, as well as hysteresis as they effloresce, especially for inorganic compositions (e.g., Santarpia et al., 2005; Tang, 1996; Zieger et al., 2014). Particles dominated by organic compounds are more likely to present more gradual hygroscopic growth with increasing RH without evident phase transition behavior (e.g., Carrico et al., 2005; Zieger et al., 2015).~~

~~Because of the chemical complexity of particles and the difficulty in measuring ~~their~~precise molecular composition and relating that to water uptake with increasing RH, it is common to use simplified parameterizations to describe the change in extinction (or scattering) with atmospheric RH relative to a dry or~~

Formatted: Font: (Default) Times New Roman, English (U.S.)

Formatted: Font: Times New Roman, Not Bold, English (U.S.)

Formatted: Heading 1

Formatted: Font: (Default) Times New Roman, English (U.S.)

Formatted: English (U.S.)

Formatted: English (U.S.)

Formatted: English (U.S.)

Formatted: English (U.S.)

Formatted: English (U.S.)

Formatted: English (U.S.)

Formatted: English (U.S.)

Formatted: English (U.S.)

Formatted: English (U.S.)

Formatted: English (U.S.)

1 low-RH state. The most frequently used of these parameterizations is a power-law function known as the
2 "gamma" parameterization, which was first used by Kasten et al. (1969). This empirically derived, single
3 parameter equation is often written as

$$4 \frac{\sigma(RH)}{\sigma(RH_0)} \equiv f(RH) = \left[\frac{(100-RH_0)}{(100-RH)} \right]^\gamma \quad (1)$$

5 where $\sigma(RH)$ is the bulk aerosol extinction at the ambient RH condition, $\sigma(RH_0)$ the extinction at the dry (low
6 RH) condition RH_0 , and γ is a parameter fitted to the observed data. The γ parameterization has been widely used
7 to describe aerosol hygroscopicity (e.g., Attwood et al., 2014; Doherty et al, 2005; Kasten, 1969; Massoli et al.,
8 2009; Quinn et al., 2005). Doherty et al. (2005) and Quinn et al. (2005) showed that in many environments the
9 value of γ varies systematically with composition, and especially with the ratio of submicron organic aerosol
10 (OA) mass to the mass of submicron sulfate plus OA. Thus one can approximately predict $f(RH)$ at arbitrary RH
11 given information on bulk submicron particle composition.

12 In this paper we examine the change in aerosol extinction at 532 nm wavelength as a function of RH based on
13 measurements from two airborne field projects in the southeastern ~~U.S.~~ US in the summer. This analysis focuses
14 on mid-day and afternoon data collected when the planetary boundary layer was fully developed because 1) prior
15 to daytime atmospheric mixing, aerosols may be chemically diverse and externally mixed, leading to complex
16 hygroscopic growth patterns that are hard to characterize (Santarpia, 2005); 2) we wish to develop an
17 understanding of aerosol hygroscopicity that is regionally representative, and the well-developed, cloud-topped
18 boundary layer structure examined here is typical of the southeastern ~~U.S.~~ US in summertime (Warren et al.,
19 1986); and 3) most of the airborne data were taken in the late morning and afternoon in fair weather. ~~By~~

20 ~~applying~~ ~~We describe the observed variability in aerosol composition, size distribution, and hygroscopicity~~
21 ~~characteristics in this environment and evaluate the suitability of~~ κ -Köhler and Mie theories to ~~these data,~~
22 ~~we represent~~ $f(RH)$. ~~We~~ develop ~~and use~~ a new single-parameter equation ~~to accurately~~ that better describe $f(RH)$.
23 ~~The relationship between~~ in this new parameter, κ_{ext} , ~~and environment than does~~ the hygroscopicity parameter κ
24 ~~from~~ κ Köhler theory is examined, and the new γ parameterization is compared to the γ power law model. (Eq.
25 1).

26 ~~—~~ ~~This paper is the second of three that analyze in detail the same airborne measurements of aerosol~~
27 ~~optical properties in the southeastern US. In a companion~~ the first paper (Wagner et al., 2015) we described in
28 ~~detail the flights, the instruments and the observations associated with vertical profiles conducted in this region.~~
29 ~~In the final~~ paper (Brock et al., 2015; ~~hereafter Part 2~~), the understanding of aerosol hygroscopicity developed
30 here and the ~~same data~~ vertical profiles analyzed in Wagner et al. (2015) are used to evaluate the sensitivity of
31 AOD to a range of aerosol and meteorological parameters. ~~Part 2 also contains details of the selection of data for~~
32 ~~the analyses in both papers and the development of representative profiles for calculation of AOD sensitivities.~~

Formatted: English (U.S.)

Formatted: English (U.S.)

Formatted: English (U.S.)

Formatted: English (U.S.)

Formatted: English (U.S.)

Formatted: English (U.S.)

Formatted: English (U.S.)

Formatted: English (U.S.)

Formatted: English (U.S.)

Formatted: English (U.S.)

Formatted: English (U.S.)

Formatted: English (U.S.)

Formatted: English (U.S.)

Formatted: English (U.S.)

Formatted: English (U.S.)

Formatted: English (U.S.)

Formatted: English (U.S.)

Formatted: English (U.S.)

Formatted: English (U.S.)

Formatted: English (U.S.)

Formatted: English (U.S.)

Formatted: English (U.S.)

Formatted: English (U.S.)

Formatted: English (U.S.)

Formatted: English (U.S.)

Formatted: English (U.S.)

Formatted: English (U.S.)

Formatted: English (U.S.)

Formatted: English (U.S.)

Formatted: English (U.S.)

2 Methods

2.1 Aircraft Instrumentation

We analyze airborne, in situ data measured during ~~vertical profiles from~~ the May-July 2013 Southeastern Nexus of Air Quality and Climate (SENEX) and the portions of the August-September 2013 Study of Emissions and Atmospheric Composition, Clouds, and Climate Coupling by Regional Surveys (SEAC⁴RS) projects that were made in the southeastern ~~U.S.~~ The SENEX project used the NOAA WP-3D aircraft (typical airspeed ~100 m s⁻¹), while the SEAC⁴RS project used the NASA DC-8 aircraft (~~~200160~~ m s⁻¹). Details of the instruments, measurements, and methodology for generating regionally representative vertical profiles of aerosol, gas-phase, and meteorological parameters are given by Wagner et al. (2015). Briefly, measurements of the composition of sub-1 μm vacuum aerodynamic diameter (approximately <0.7 μm physical diameter) non-refractory particles were made by aerosol mass spectrometers (AMS, Aerodyne, Billerica, Massachusetts, ~~USAUS~~; Canagaratna et al., 2007; DeCarlo et al., 2006) each with extensive customization for aircraft use (~~Bahreini et al., 2008; Dunlea et al., 2009; Middlebrook et al., 2012~~). The AMS used during SENEX employed a compact time-of-flight mass spectrometer (~~CTOFC-ToF~~) while that used during SEAC⁴RS employed a high-resolution time-of-flight mass spectrometer with greater resolving power (~~HRTOFHR-ToF~~, DeCarlo et al., 2006). The mass of black carbon (BC) particles was measured on both projects with the same humidified tandem single-particle soot photometer (SP2; Droplet Measurement Technologies, Boulder, CO, ~~USAUS~~; Schwarz et al., 2015). Dry particle size distributions from ~0.07 to 1.0 μm were measured with two separate ultra-high sensitivity aerosol size spectrometers (UHSAS, Particle Metrics, Inc., Boulder, Colorado, ~~U.S.;US~~; Brock et al., 2011; Cai et al., 2008), one on each project. Aerosol extinction at 532nm wavelength and three relative humidities (~15%, ~70%, and ~90%) was measured simultaneously with a custom built multichannel cavity ringdown spectrometer (CRDS; Langridge et al., 2011) on both projects.

Air entering the CRDS passed through a 40cm long carbon monolith denuder (210cpi/30mm OD, MAST Carbon, Basingstoke, United Kingdom) to remove semivolatile inorganic and organic gases. The flow was then dried to a low RH (~~usually <~15% and always <25%, range 8-24%~~), below the efflorescence point of atmospherically relevant salts, using multitube Nafion dryers (PD-200T-12MSS, Permapure Inc., Toms River, New Jersey, ~~U.S.;US~~) with a sample residence time of 0.25 s. For measurement by the two elevated RH channels, the sample was humidified to >90% RH by cooling the sample flow inside Nafion humidifiers (MH-110-12-S-4, Permapure Inc., Toms River, New Jersey, ~~U.S.;US~~), causing deliquescence. The sample flow was then reheated to the ~~temperature~~ temperatures of the measurement cells in the instrument, which were controlled using RH sensors (Model HMP110, Vaisala Inc., Helsinki, Finland) to achieve the desired measurement RH. Typically, one ~~elevated-RH~~ channel measured at ~70% RH (~~actual range 70-73%~~) and the other measured at ~90% RH (~~actual range 86-94%~~). ~~Data were excluded from analysis when the RH of high-RH channel was <85%.~~

~~Histograms of measured RH values for each CRDS channel are given in the Supplemental Materials.~~ The cooling in the humidifiers was 10-15K and 1-3K below the cell temperatures of the medium- and high-RH channels respectively. Total time of exposure to elevated humidities was ~4s, of which 0.4 s was in the cooled section and 3.6 s was in the warmed section. Calculated and measured $f(RH)$ for 300nm ammonium sulfate

Formatted: Font: (Default) Times New Roman, English (U.S.)

Formatted: Font: Times New Roman, Not Bold, English (U.S.)

Formatted: Heading 1

Formatted: Font: (Default) Times New Roman, English (U.S.)

Formatted: Font: (Default) Times New Roman, English (U.S.)

Formatted: Heading 2, Space Before: 0 pt, After: 0 pt

Formatted: Font: (Default) Times New Roman, English (U.S.)

Formatted: Font: Times New Roman, Not Bold, English (U.S.)

Formatted: English (U.S.)

Formatted: English (U.S.)

Formatted: English (U.S.)

Formatted: English (U.S.)

Formatted: English (U.S.)

Formatted: English (U.S.)

Formatted: English (U.S.), Superscript

Formatted: English (U.S.)

Formatted: English (U.S.)

Formatted: English (U.S.)

Formatted: English (U.S.)

Formatted: English (U.S.)

Formatted: English (U.S.)

Formatted: English (U.S.)

Formatted: English (U.S.)

Formatted: English (U.S.)

Formatted: English (U.S.)

Formatted: English (U.S.)

Formatted: English (U.S.)

1 particles are in agreement within uncertainties (Langridge et al., 2011), indicating that the humidified residence
2 time is sufficient to allow hygroscopic particles to grow to equilibrium. However, the instrument has not been
3 tested with less hygroscopic organic particles that might exhibit kinetic limitations to water uptake. This remains
4 an uncharacterized uncertainty.

5 ~~The changes in sample temperature in the inlet, sample line, humidifiers, and CRDS cells may lead to loss of~~
6 ~~semi-volatile species; these possible effects are ignored. Condensation of semi-volatile compounds is excluded~~
7 ~~by the upstream denuder. Submicron ammonium nitrate was $<0.04 \mu\text{g m}^{-3}$ in the daytime during~~
8 ~~contemporaneous measurements at a ground site in Centreville, Alabama in June 2013 (Attwood et al., 2014;~~
9 ~~Guo et al., 2015). The upstream denuder excludes condensation of semi-volatile compounds.~~ Because of the
10 initial high level of humidification prior to reheating, the CRDS measurements at elevated RH were made on the
11 metastable (humidified) branch of any deliquescence/efflorescence hysteresis curve. This better represents the
12 likely state of the aged atmospheric aerosol in the cloud-topped planetary boundary layer than would
13 measurements made on the deliquescence branch of the curve. We did not attempt to measure aerosol extinction
14 at ambient humidity because it is difficult to regulate instrument humidity rapidly enough to respond to ambient
15 RH changes in flight.

16 ~~The CRDS optical extinction measurements were made behind an impactor with a 50% efficiency at 1.0 μm~~
17 ~~aerodynamic diameter. Accounting for particle and air density, typical 50% impactor efficiency was $\sim 0.7 \mu\text{m}$~~
18 ~~physical diameter at the inlet RH, which was measured at $<50\%$ during SENEX due to dynamic heating during~~
19 ~~sampling, and was presumably lower during SEAC⁴RS due to the higher aircraft speed. Coarse ($>0.7 \mu\text{m}$)~~
20 ~~particle size distributions were measured during SENEX with a custom built white light optical particle counter~~
21 ~~at $<50\%$ RH conditions (Brock et al., 2011), allowing calculation of coarse particle extinction. The contribution~~
22 ~~to extinction due to dry coarse particles was estimated using Mie theory and an assumed refractive index of~~
23 ~~$1.59+0i$ (that of the polystyrene latex (PSL) sphere calibrant), and was on average $<7\%$ of the total calculated~~
24 ~~extinction for the data measured in the planetary boundary layer. We ignore the contribution to extinction for~~
25 ~~particles larger than $0.7 \mu\text{m}$ physical diameter in the remainder of this work. Based on the known particle~~
26 ~~transmission characteristics of the AMS inlet and the measured size distribution, the AMS was estimated to~~
27 ~~sample $>97\%$ of the sub $0.7 \mu\text{m}$ particle volume (Wagner et al., 2015); the AMS, CRDS, SP2, and UHSAS all~~
28 ~~comparably and quantitatively sampled the sub $0.7 \mu\text{m}$ aerosol.~~

29 **2.2**—~~A low-turbulence inlet and sampling system (Brock et al., 2011) was used during SENEX. During this~~
30 ~~project the AMS, CRDS, SP2, and UHSAS sampled downstream of an impactor with 50% efficiency at 1.0 μm~~
31 ~~aerodynamic diameter (PM1). Accounting for particle and air density, typical 50% impactor efficiency was ~ 0.7~~
32 ~~μm physical diameter at the inlet RH, which was measured at $<50\%$ due to dynamic heating during sampling.~~
33 ~~Particle losses in the CRDS system were characterized experimentally by Langridge et al. (2011) using particles~~
34 ~~size-selected with a custom-built differential mobility analyzer (DMA) of the design now available~~
35 ~~commercially (Brechtel Manufacturing, Inc., Hayward, CA, US). Losses within the instrument were $<1.25\%$ for~~
36 ~~submicron particles at RH values up to 92%. Transmission of 0.1- $0.7 \mu\text{m}$ particles in the turbulent transmission~~
37 ~~line (inner diameter 0.95 cm, length 3 m, flowrate 20 l min^{-1}) between the impactor and the AMS, CRDS, SP2,~~
38 ~~and UHSAS was calculated for inertial, gravitational, and diffusive losses using the aerocalc.xls spreadsheet~~
39 ~~(Baron, 2001) and was >0.992 for the range of flight conditions encountered. Based on the known particle~~

Formatted: English (U.S.)

Formatted: English (U.S.)

1 transmission characteristics of the AMS focusing lens inlet and the measured size distribution, the AMS was
2 estimated to sample >97% of PM1 particle volume (Wagner et al., 2015). During SEAC⁴RS, the aerosol
3 instruments sampled ambient air using a shrouded conical diffusing inlet that transmitted particles smaller than
4 2.8 μm aerodynamic diameter with efficiency >95% (McNaughton et al., 2007). The CRDS and UHSAS
5 sampled downstream of the same 1.0 μm impactor used in SENEX. Calculated particle transmission through the
6 tubing between the inlet and the CRDS and UHSAS instruments was >0.99. The AMS, CRDS, SP2, and
7 UHSAS all comparably and quantitatively sampled PM1 aerosol during both SENEX and SEAC⁴RS.

8 The accuracy of the $f(RH)$ measurement made by the CRDS instrument was reported in Langridge et al. (2011)
9 using ammonium sulfate particles size selected with a differential mobility analyzer (DMA) as an
10 atmospherically relevant model hygroscopic aerosol and PSL as a model hydrophobic aerosol. The accuracy of
11 $f(RH)$ determined by this approach was within $\pm 2\%$ (at $RH=76\%$) and $\pm 14\%$ (at $RH=95\%$) of values calculated
12 by κ -Köhler theory, well within experimental uncertainty. The optical power in the sample cells of the CRDS is
13 much less than the 40-100 mW lasers that illuminate the optical cavities, and the aerosol is not measurably
14 heated. The humidity is controlled by direct measurement of RH within each ringdown cell. Because the CRDS
15 provides a fundamental measurement of extinction, repeated extinction calibrations are not necessary. The gas-
16 phase extinction measurement was periodically checked with an ozone source measured by an independent
17 ozone sensor (Thermo Environmental Instruments, Model 49i Ozone Analyzer) and showed no systematic biases
18 in the CRDS extinction during SENEX or SEAC⁴RS. The probes measuring the RH of the sample cells (Vaisala
19 HMP110) were calibrated before and after the SENEX and SEAC⁴RS missions using the equilibrium water
20 vapor pressure over salt solutions (Vaisala HMK15) providing nominal RH values of 33% (MgCl_2), 75%
21 (NaCl), and 97% (K_2SO_4). The RH values reported by probes were within the manufacturer's stated uncertainty
22 of $\pm 2\%$ for $RH < 90\%$ and $\pm 3\%$ for $RH > 90\%$ for these salt solutions. The total accuracy in the 1-s humidified
23 extinction measurement is estimated to be $\pm 5\%$, $\pm 10\%$, and $\pm 15\%$ at $\sim 15\%$, $\sim 70\%$, and $\sim 90\%$ RH, respectively. Thus
24 the uncertainty in $f(RH)$ is estimated to be $\pm 11\%$ and $\pm 16\%$ for the medium and high RH channels, respectively.
25 This uncertainty estimate does not account for possible residual water present in particles in the $\sim 15\%$ RH
26 channel, which could bias the $f(RH)$ values low.

27 **2.2 Corrections to UHSAS size distributions for refractive index**

28 The size distribution reported by the UHSAS is a function of the amount of light scattered onto the instrument's
29 photodetectors, and the quantity of scattered light is itself a function of the composition-dependent aerosol
30 refractive index. Hence, it is necessary to correct the measured UHSAS size distributions for changing aerosol
31 composition during flight. This correction was accomplished by first calibrating the instrument to an aerosol of
32 known refractive index to relate scattering amplitude to discrete pulse height channels. Next, the Mie scattering
33 over the optical geometry of the instrument was calculated to determine how each channel was related to particle
34 diameter for an atmospherically relevant range of real refractive index. Finally, a look-up table of this
35 relationship was used to determine the actual diameter represented by each channel as refractive index,
36 calculated from the AMS measurements as described in Section 2.3, varied. The UHSAS exhibits a monotonic
37 response function for submicron particles (Cai et al., 2008).

Formatted: Font: (Default) Times New Roman, English (U.S.)

Formatted: Heading 2, Space Before: 0 pt, After: 0 pt

Formatted: Font: Times New Roman, Not Bold, English (U.S.)

Formatted: English (U.S.)

Formatted: English (U.S.)

1 The UHSAS operated during SENEX was calibrated using atomized, dried ammonium sulfate particles sized
2 with ~~a custom-built differential mobility analyzer (DMA) of the design now available commercially (Brechtel~~
3 ~~Manufacturing, Inc., Hayward, CA, U.S.)~~ ~~the DMA previously described.~~ The sizing accuracy of the DMA was
4 better than 2% as determined using NIST-traceable PSL microspheres in eight sizes from 0.1 to 1.2 μm (Thermo
5 Fisher Scientific, Inc., Waltham, MA, ~~U.S.)~~ ~~US).~~ The UHSAS was calibrated on five days with >36 separate
6 ammonium sulfate particle sizes during the SENEX mission, in addition to pre-flight daily calibration checks
7 using four PSL microsphere sizes. The UHSAS that was operated by the NASA Langley group during SEAC⁴RS
8 was calibrated using PSL microspheres and the calibration was checked twice during each flight by generating
9 an aerosol containing four microsphere sizes and introducing it into the inlet sample flow as the aircraft was
10 flying.

Formatted: English (U.S.)

Formatted: English (U.S.)

11 The response of the UHSAS was simulated using numerical Mie calculations (Bohren and Huffman, 1983) of
12 the light scattered over the solid angle that is imaged onto the instrument's photodetectors. Assumptions include
13 spherical, homogeneous particles with composition that is invariant with particle diameter. The geometry of the
14 detection optics was determined from a review of technical drawings with the manufacturer. Light is scattered
15 perpendicularly to the beam from a neodymium-doped yttrium lithium fluoride laser (1053 nm) and is imaged
16 onto solid state photodetectors on each side of the scattering cell using pairs of Mangin mirrors in clamshell
17 configurations. The signal from each detector is amplified through two gain stages, for a total of four
18 independent gain stages. Each detector samples the light scattered by particles over a circularly symmetric angle
19 from 33-147°. The center region of the angle, between 75.2 and 104.8° is not sampled because of the hole cut in
20 the outer of the Mangin mirrors (the detector area is a negligible fraction of this hole area). Thus the imaged
21 solid angle is a conical annulus. This geometry is consistent with that reported by Petzold et al. (2013), but
22 ~~contrasts with that reported for the UHSAS by Cai et al., (2008), who appear to have incorrectly used a 22-158°~~
23 ~~scattering angle to simulate UHSAS instrument response, but is consistent with that reported by Petzold et al.~~
24 ~~(2013).~~

Formatted: English (U.S.)

Formatted: English (U.S.)

25 Using the calibrations, the relationship between the 99 size channels and the amount of light scattered onto the
26 detectors was determined. Knowing that each channel represents a certain amount of scattered light, the Mie
27 model was used to calculate the particle diameter corresponding to each channel for a range of particle real
28 refractive indices from 1.40 to 1.60, in increments of 0.01, producing a look-up table relating channel number to
29 particle diameter as a function of real refractive index. Using the AMS data and the composition model
30 described in Section 2.3, the real refractive index was determined by volume-weighted averaging for each AMS
31 data point using the values in Table 1. The mean and standard deviation of the real part of the calculated
32 refractive index was 1.547 ± 0.004 for the data analyzed here. Using the real refractive index for each point, the
33 look-up table was then applied to determine the physical diameter for each UHSAS channel for each
34 measurement interval. Residual water content in the dry (~~25~~ ~~(~15~~ RH) aerosol was not considered. The
35 variation in instrument response due to the imaginary component of the refractive index, k , also was not
36 considered. Because BC concentrations measured by the SP2 were very low (averaging $<0.05 \mu\text{g m}^{-3}$ for the data
37 analyzed here), k was calculated to be 0.006 ± 0.004 , and thus was ignored in the generation of the UHSAS look-
38 up table. However, the BC component was included in the calculation of κ_{chem} , refractive index, and extinction as
39 described in Section 2.3 below.

Formatted: English (U.S.)

Formatted: English (U.S.)

Formatted: English (U.S.)

2.3 Method to calculate ambient extinction

To determine ambient extinction, measurements of extinction made at three discrete RH values of ~15%, ~70%, and ~90% may be interpolated or extrapolated to ambient conditions at arbitrary RH based on a parametric model such as the γ function. However, because the measurements analyzed here include submicron aerosol size distributions and composition, a more explicit and accurate method to determine ambient extinction can also be used (Fig. 1a). Petters and Kreidenweis (2007) proposed the κ -Köhler parameterization that describes the water activity of an aqueous solution without considering explicitly the effect of individual ionic components. The κ -Köhler approach has been used widely to predict subsaturated particle growth as well as the activation of cloud condensation nuclei (CCN). Ignoring curvature effects for particles diameters >100 nm, the hygroscopic growth of a water-soluble aerosol can be approximated as

$$gf_{diam} \cong \left(1 + \kappa_{chem} \frac{RH}{100 - RH}\right)^{1/3} \quad (2)$$

where gf_{diam} is the diameter growth factor, the ratio of the particle's wet diameter to its dry diameter. An equation of this form was first used by Rissler et al. (2006) to describe observed hygroscopic growth factors. The parameter value of κ_{chem} for a mixed particle composition may be calculated from the volume-weighted contribution due to average of the κ_{chem} of each species i , κ_i , which contributes to the aerosol composition:

$$\kappa_{chem} = \frac{\sum_i (\kappa_i X_i / \rho_i)}{\sum_i (X_i / \rho_i)} \quad (3)$$

where X_i is the mass concentration and ρ_i the dry density of species i . The κ_i are determined from thermodynamic model calculations or by experimentally determining the growth factors for individual compounds, as

$$\kappa_{chem} = \frac{\sum_i (\kappa_i X_i / \rho_i)}{\sum_i (X_i / \rho_i)} \quad (3)$$

where X_i is the mass concentration and ρ_i the dry density of species i . This volume-weighted approach follows the Zdanovskii-Stokes-Robinson (Stokes and Robinson, 1966) mixing rule, which states that each component of the mixture acts independently and that the optical properties are linearly additive. The accuracy of the particle diameter growth factor calculated using κ_{chem} determined from Eq. (3) varies depending on the specifics of the aerosol composition and mixing state and on the accuracy of the κ_i , but is generally observed to be better than 30% (Petters and Kreidenweis, 2007).

Using the methodology shown schematically in Fig. 1a, the measurements of aerosol composition and size distribution were used to calculate the extinction expected at the dry, medium, and high RH values measured in the CRDS. This calculation serves two purposes: it evaluates the closure of the optical, chemical, and size distribution measurements, and it helps evaluate/determine how well the γ parameterization, Eq. (1), describes $f(RH)$ in the southeastern U.S. The AMS measured the mass concentrations of sulfate, nitrate, chloride, ammonium, and OA. From these measurements, an electrolyte composition model (Zaveri, 2005) was used to calculate the concentrations of ammonium sulfate, ammonium bisulfate, letovicite, sulfuric acid, ammonium nitrate, ammonium chloride, nitric acid, and hydrochloric acid. Contributions from ions associated with electrolytes of magnesium and sodium are likely to be insignificant contributors to the submicron aerosol mass

Formatted: Font: (Default) Times New Roman, English (U.S.)

Formatted: Heading 2

Formatted

Formatted

Formatted

Formatted

Formatted

Formatted: English (U.S.)

Formatted

Formatted

1 in the continental boundary layer (Washenfelder et al., 2015). Organosulfates were estimated to contribute <4%
 2 to the submicron aerosol mass and therefore are not considered (Liao et al., 2015). The contribution of
 3 particulate organic nitrates (pON) to measured nitrate has been estimated using the method described in Fry et al
 4 (2013, 2009) for the SEAC⁴RS flights on which the HRTOFHR-ToF-AMS was operated (Day et al., 2015). The
 5 pON, likely in the form of oxidized monoterpene nitrates (Boyd et al., 2015; Draper et al., 2015; Xu et al.,
 6 2015a,b) is estimated to be between 15 and 40% of the total measured nitrate above the surface in the well-
 7 mixed and transition layers, and more than 63% across the southeastern U.S-US at the surface (Xu et al., 2015a).
 8 However, nitrate represented <5% of fine aerosol mass in the data analyzed here. Lacking specific information
 9 on pON density or hygroscopicity, and given its relatively small contribution to aerosol mass in summer (<12%
 10 of OA and <8% of submicron mass; Xu et al., 2015b), all measured nitrate is treated as ammonium nitrate.
 11 Finally, potential phase separation phenomena that have been found in laboratory studies of OA/inorganic
 12 mixtures (e.g., Hodas et al., 2015), insoluble inclusions that might influence hygroscopicity (Pringle et al.,
 13 2010), and the diameter dependence of κ_{chem} discussed by Good et al. (2010a) are ignored.

14 The bulk aerosol κ_{chem} was determined from the volume-weighted κ_i values (Table 1) using Eq. (3). Aerosol
 15 extinction at the measured low, medium and high humidities was then calculated as follows (Fig. 1a). First, as
 16 detailed in Section 2.2., the optically equivalent dry diameters measured by the UHSAS were converted into
 17 physical dry diameters, accounting for the effects of varying composition on the real refractive index, which
 18 varied only slightly (interdecile range 1.54-1.56). Next, the particle diameter at the ambient RH, D_{RH} , was
 19 calculated using κ -Köhler theory (including the Kelvin effect) by numerically solving

$$\frac{RH}{100} = \frac{D_{RH}^3 - D_d^3}{D_{RH}^3 - D_d^3(1 - \kappa_{chem})} \exp\left(\frac{4\sigma_s M_w}{RT\rho_w D_{RH}}\right) \quad (4)$$

21 where D_d is the dry diameter, σ_s the surface tension of water at the particle/air interface, and M_w and ρ_w the
 22 molecular weight and density of water, respectively (Petters and Kreidenweis, 2007). Finally, Mie theory
 23 (Bohren and Huffman, 1983) was used to calculate the expected extinction coefficient, σ_{ext} , at the ambient RH
 24 using the water-swelled D_{RH} and water-corrected, volume-weighted refractive index n , as

$$\sigma_{ext} = \int_{A}^{700 \text{ nm}} \frac{\pi}{4} D_{RH}^2 \alpha(D_{RH}, n) N(D_{RH}) dD_{RH}, \quad (5)$$

26 where α is the extinction efficiency and N the number concentration of particles in diameter interval dD_{RH} .

27 In calculating ambient extinction using Eq. (5) it is assumed that there is no size dependence to κ_{chem} ; instead it is
 28 assumed that all optically active particles are spherical, internally mixed and have the same composition
 29 regardless of size. This assumption is supported qualitatively by inspection of the size-dependent composition
 30 periodically measured by the AMS instruments. The differences in the real refractive index between the UHSAS
 31 sensing laser (1053 nm) and the humidified CRDS (532 nm) wavelengths of about 0.02 (Toon et al., 1976) are
 32 not considered. We also ignore the contribution of submicron soil components, which were not separately
 33 measured but whose concentrations measured at a surface site nearby were negligible (Washenfelder et al.,
 34 2015), and of sea-salt, which has low concentrations in the southeastern US in summer (Guo et al., 2015).

Formatted

Formatted

Formatted

Formatted

Formatted

Formatted: English (U.S.)

2.4 Uncertainty in calculated and measured extinction

Extinctions were calculated from the measured composition and the UHSAS size distributions for the low (25 ~15% RH) medium (~70% RH) and high (~90% RH) conditions of measurement in the CRDS instrument.

The uncertainties in these extinctions are difficult to estimate because of the multiple steps of processing (Fig. 1a), including modeling the UHSAS instrument response, and the assumptions inherent in the calculation (e.g., internally mixed, homogeneous, spherical particles). We assume that κ_{chem} for inorganic electrolytes can be estimated to within ~20%, based on ranges found in the cited literature. This uncertainty includes the uncertainty in the composition determined by the AMS. This uncertainty may appear low, since AMS accuracy for absolute concentrations is ~35%, driven in large part by uncertainties in particle collection efficiency (Middlebrook et al., 2012). However, only the mass fractions of the individual aerosol constituents are used when calculating κ_{chem} , so the collection efficiency does not contribute to the uncertainty assuming that all components of a particle are collected with the same efficiency. Instead, the uncertainty is dominated by other factors such as relative ionization efficiency for different compounds, and is taken to be ~20%; this uncertainty is an area of current research: (Murphy et al., 2016). For OA, the uncertainty in the κ_{chem} is much larger because the OA composition is largely unknown. Values of κ_{chem} for various OA compositions measured in the laboratory vary from 0 to 0.5 (e.g., Petters and Kreidenweis, 2007; Rickards et al., 2013). To achieve consistency with the observed $f(RH)$, we have chosen a κ_{chem} for OA, $\kappa_{chem,org}$ of 0.076050. The range of $\kappa_{chem,org}$ values that are consistent with our observations within uncertainties is discussed further in Section 3.43.

The uncertainty in the size distribution measured by the UHSAS has been examined in detail elsewhere (see Supplemental Material in Cai et al., 2008; Brock et al., 2011). For particle diameters <0.5 μm , and an assumed a range in real refractive index of 1.43-1.56 with negligible absorption, the actual diameter may deviate by up to 8% from the reported diameter, which is based on ammonium sulfate calibration. However, because we correct the size distribution for refractive index effects as described in Section 2.2, the error in the diameters used to calculate extinction is estimated to be <3% based on calibration precision. Concentration uncertainty due to counting statistics is <4% for the cases analyzed here, and that due to the sample flow measurement is <1.6%. ~~The absolute uncertainty in the measurement of the instrumental RH is $\pm 2\%$, increasing to $\pm 3\%$ for RH values exceeding 90%.~~

The uncertainties described above propagate to extinction nonlinearly through the κ -Köhler equation (Eq. (4)) and through the Mie calculation (Eq. (5)). We use a Monte Carlo approach to simulate the expected uncertainty in the extinction determined at the three relative humidities. Three values each of geometric mean diameter, geometric standard deviation, and κ_{chem} were chosen spanning the interdecile range of observed values, creating a total of 27 cases. For each case, the extinction at the three RH values was calculated, as described in Section 2.3 (Fig. 1a), 1000 times while median diameter, standard deviation, κ_{chem} , and RH each was simultaneously varied by a normally-distributed random error corresponding to the uncertainty in that parameter. In addition, a normally-distributed random uncertainty was added to represent counting statistics and flow uncertainty. The resulting total relative errors for calculated extinction varied only slightly as function of extinction, with a mean relative error of $\pm 34\%$. This value is used as the best estimate of total uncertainty in calculated ambient extinction.

Formatted: Font: (Default) Times New Roman, English (U.S.)

Formatted: Font: Times New Roman, Not Bold, English (U.S.)

Formatted: Heading 2

Formatted: Font: (Default) Times New Roman, English (U.S.)

Formatted: English (U.S.)

Formatted: English (U.S.)

Formatted: English (U.S.)

Formatted: English (U.S.)

Formatted: English (U.S.)

Formatted: English (U.S.)

Formatted: English (U.S.)

1 The calibration accuracy in directly-measured CRDS extinction varies with measurement RH, and is $\pm 2\%$ at
2 $\leq 25\%$ RH, $\pm 5\%$ at $\sim 70\%$ RH, and $\pm 15\%$ at $\sim 90\%$ RH for extinction values exceeding 20 Mm^{-1} . Instrument
3 precision for 1-s data is $\pm 5\%$ at 50 Mm^{-1} .

4 For the seven flights analyzed for this study, the extinction calculated from the AMS and size distribution data
5 (Section 2.3) and the extinction measured by the CRDS agreed within the combined experimental uncertainty at
6 all three measurement humidities (Table 2, Fig. 2). During the SEAC⁴RS flight of 6 September 2013, the
7 UHSAS did not function, so ~~data for this flight extinction was not calculated from a laser aerosol spectrometer~~
8 ~~(LAS, TSI, Inc., St. Paul, MN, U.S.) were used for the size distributions instead. We do not have an instrument~~
9 ~~model with which to correct the reported LAS composition and size distribution, calibrated using PSL~~
10 ~~microspheres, for refractive index effects. The calculated low RH measurements, although the extinction values~~
11 ~~for this flight were 38% lower than the measured values. However, the calculated and measured $f(RH)$ showed~~
12 ~~no substantial bias for this flight, which suggests a LAS concentration error rather than a bias in measured~~
13 ~~particle diameter. Because this flight was one of only two from late summer contributing to the analyzed dataset,~~
14 ~~to improve seasonal representativeness the data from this flight directly by CRDS, are included in the analysis~~
15 ~~despite the differences in instrumentation used.~~

16 All aerosol data used in this analysis have been corrected to conditions of 1013 hPa and 273.15 K. All aerosol
17 data were measured at 1 s intervals, with the exception of the C-ToF-AMS measurements during SENEX, which
18 were made over 10 s intervals. When calculating extinction from the AMS and size distributions (Fig. 1a), the
19 SENEX data were averaged to match the C-ToF-AMS measurement frequency. The SEAC⁴RS data, including
20 that from the HR-ToF-AMS, were averaged to 10s to maintain statistical consistency with the SENEX data.

21 **3. Results and analysis**

22 In this section we describe the observed aerosol properties and their vertical structure, explore the relationship
23 between particle composition and hygroscopicity, place constraints on the hygroscopicity of the OA component
24 of the submicron aerosol, and present a new parameterization to describe the $f(RH)$ curve.

25 **3.1 Selection of data**

26 This analysis focuses on in situ measurements obtained during vertical profiles from the SENEX and SEAC⁴RS
27 flights made in the southeastern states of Louisiana, Mississippi, and Georgia (Fig. 2). These data were selected
28 because they were the focus of analysis by Wagner et al. (2015) of particle vertical mixing and mass production,
29 and because the results of this analysis and these profiles are used in a companion paper evaluating the
30 sensitivity of AOD to several aerosol parameters and to RH (Brock et al., 2015). Wagner et al. (2015) describe in
31 detail the selection criteria for the profiles. Briefly, profiles were included in the analysis if they were in the
32 afternoon during fair-weather cumulus conditions, exhibited a well-mixed layer between the surface and cloud
33 base, and contained a distinct transition (cloud) layer between the well-mixed layer and the free troposphere
34 above. The optical well-mixed and transition layers were defined on the basis of the oxidation lifetime of the gas-
35 phase species CO and isoprene. Air within the well-mixed layer was in immediate (< 1 hr) contact with surface

Formatted: English (U.S.)

Formatted: English (U.S.)

Formatted: English (U.S.)

Formatted: English (U.S.)

Formatted: English (U.S.)

Formatted: English (U.S.), Superscript

Formatted: English (U.S.)

Formatted: English (U.S.)

Formatted: English (U.S.)

Formatted: English (U.S.)

Formatted: English (U.S.)

Formatted: English (U.S.)

Formatted: English (U.S.)

Formatted: English (U.S.)

Formatted: Font: (Default) Times New Roman, English (U.S.)

Formatted: Heading 1, Space Before: 0 pt, After: 0 pt

Formatted: Font: Times New Roman, Not Bold, English (U.S.)

Formatted: English (U.S.)

1 isoprene emission, while the transition layer was evidently a result of mixing between the well-mixed layer and
2 the free troposphere over time scales of hours.

3 Of the 74 profiles made in the geographic area of interest, 37 met the criteria of Wagner et al. (2015) and 25 met
4 both the meteorological criterion and the criterion that the high RH channel be at $RH < 85\%$. The aircraft flight
5 tracks and locations of these profiles are shown in Fig. 2. Brock et al. (2015) show that the AOD values
6 calculated by vertically integrating the ambient extinction ~~of~~ derived from the in situ measurements in the
7 profiles are regionally representative and are consistent with ground-based climatologies of AOD determined
8 from sunphotometer measurements. Thus the measurements presented here are typical of the daytime,
9 summertime, daytime background and moderately polluted rural aerosol in the cloud-topped boundary layer of
10 the southeastern U.S. ~~was~~ this region.

11 3.2 Observed aerosol composition and hygroscopicity

12 Data from a single example profile, measured at three RH values (Fig. 2). At the medium (~70%) RH, the optical
13 in east central Alabama on 20130622 are shown in Fig. 3. The measured extinction was higher than at the low-
14 RH-, medium, and high RH values (Fig. 3a), along with the RH values measured in the CRD cells and ambient
15 air (Fig. 3b) are the fundamental measurements. The $f(RH)$ values from the medium and high RH channels are
16 shown in Fig 3c. Within the well-mixed layer the dry extinction by a factor of only ~1 to 1.5. At the high (~was
17 nearly constant (Fig. 3a). The ambient RH reached a maximum at the top of the well-mixed layer (Fig. 3b),
18 where the bases of the fair-weather cumulus clouds were typically found. The fraction of PM1 dry mass that was
19 measured by the AMS to be inorganic was ~0.3 in the well-mixed and transition layers, and increased to ~0.55 in
20 the free troposphere. Because inorganic compounds are generally more hygroscopic than organic species
21 (e.g., Petters and Kreidenweis, 2007), the $f(RH)$ at ~90% RH, the aerosol displayed a much wider range of
22 $f(RH)$ values, varying from ~1.2 to 3.5, with a modal value of ~1.8 (Fig. 3).
23 in the well-mixed and transition layers to >2.5 in the free troposphere. For comparison, the $f(RH)$ for pure 300nm
24 ammonium sulfate particles at 532nm wavelength is expected to be ~2 at 70% RH and ~4 at 90% RH (Langridge
25 et al., 2011). InBecause the following sections we develop a new parameterization to describe the $f(RH)$ curve,
26 explore extinction and mass of the aerosol within the relationship between particle free troposphere was only
27 ~15% of that within the well-mixed layer, the well-mixed layer aerosol dominated aerosol composition and this
28 parameterization, and place constraints on the hygroscopicity of the OA component of within the submicron
29 aerosol transition layer.

30 3.1 Parameterizing $f(RH)$

31 The hygroscopic growth of particles and $f(RH)$ can be calculated using the technique shown in Fig. 1a. However,
32 a simplified parameterization based on optical measurements alone (Fig. 1b) is useful when compositional or
33 size distribution observations are not available. The often used γ parameterization (Eq. (1)) has the desired
34 simplicity; however, as shown in Fig. 4a, it does not produce a hygroscopic growth curve that matches the $f(RH)$
35 directly observed or calculated from the composition and size distribution measurements used in this analysis.
36 Values of γ fitted to both the $f(RH)$ data (Fig. 4a), overpredict observed $f(RH)$ at 70% RH. The planetary
37 boundary layer in the southeastern U.S. is often at humidities between 50 and 90% where the γ parameterization

Formatted: English (U.S.)

Formatted: English (U.S.)

Formatted: English (U.S.)

Formatted: English (U.S.)

Formatted: English (U.S.)

Formatted: English (U.S.)

Formatted: English (U.S.)

Formatted: English (U.S.)

Formatted: English (U.S.)

Formatted: English (U.S.)

Formatted: English (U.S.)

Formatted: English (U.S.)

Formatted: English (U.S.)

Formatted: English (U.S.)

Formatted: English (U.S.)

Formatted: English (U.S.)

Formatted: English (U.S.)

Formatted: English (U.S.)

Formatted: English (U.S.)

Formatted: English (U.S.)

could lead to overprediction of the ambient extinction by 20% or more. Because of these biases we have sought a different single parameter representation of the $f(RH)$ curve.

We use κ -Köhler theory to develop an alternative parameterization for $f(RH)$. The cube of the diameter growth factor gf_{vol} (Eq. (2)) is the volume growth factor. Relating the volume growth factor to bulk $f(RH)$ however, involves the complicated variation of aerosol extinction efficiency as a function of particle diameter, often described using Mie theory. As particles grow due to water uptake as RH increases, the extinction cross section can change non-linearly, and can even decrease (e.g., Bohren and Huffman, 1983). However, as pointed out earlier (Chylek, 1978; Pinnick et al., 1980), for a physically realistic, polydisperse aerosol composed of particles predominantly smaller than the wavelength of light (but larger than Rayleigh scatterers), σ_{ext} is roughly proportional to integrated particle volume or mass. This proportionality results because the extinction efficiency $Q_{ext}(D_p, m)$ for visible light can be approximated as a linear function of particle diameter over the relatively broad size range of a polydisperse accumulation mode atmospheric aerosol (i.e., Q_{ext} is proportional to D_p , Fig. 5). If this is true, it follows from Eq. (5) that $\sigma_{ext} \propto D_p^3$ extinction is proportional to volume. Thus the relative change in extinction, $f(RH)$, is roughly proportional to the relative change in volume, which for the case of a deliquescing aerosol is the volume growth factor gf_{vol} . This proportionality applies for an aerosol of constant refractive index, which is not the case for an atmospheric aerosol particle growing by addition of water with increasing RH (Hegg et al., 1993; Hänel, 1976). This ~20% effect on $f(RH)$ due to refractive index change for RH \leq 90% (Hegg et al., 1993) can be ignored to first order. The approximate proportionality between extinction and volume is valid for particles smaller than the wavelength of light, which for these measurements is 522 nm. The 10th to 90th percentile range for the geometric median diameters considered here was 120–170 nm, so this approximation is valid, even for particles at high RH. The approximate (no Kelvin effect) diameter growth factor from κ Köhler theory is given in Eq. (2). The cube of this this is then roughly proportional to gf_{vol} and $f(RH)$:

$$gf_{vol} \propto f(RH) \cong 1 + \kappa_{ext} \frac{RH}{100 - RH} \quad (6)$$

where κ_{ext} is a dimensionless parameter fitted to observed $f(RH)$. When fitted to the three point $f(RH)$ measurements in SENEX and SEAC⁴RS, both the κ_{ext} and γ parameterizations describe the high RH condition well (Fig. 4a). However, the κ_{ext} parameterization predicts the medium RH extinction values better than does the γ parameterization. This improved performance is shown Fig. 4b, where the fitted and measured $f(RH)$ values at the medium (70%) RH condition for the two parameterizations are compared. The ratio of fitted to measured medium RH $f(RH)$ values for κ_{ext} is centered near 1 and is symmetric, while that for γ is >1 . Further, there are distinct differences in the fitted $f(RH)$ curves for the two approaches for RH $>$ 90%, with the κ_{ext} parameterization showing a more rapid increase in $f(RH)$ with increasing RH for these high humidity conditions. Preliminary evaluation of ambient atmospheric data acquired in winter 2015 in Boulder, Colorado, U.S. (not shown) confirms that the κ_{ext} curve more closely follows the observed $f(RH)$ for ambient particles at RH $>$ 90% than does the γ parameterization.

In summary, the power law γ parameterization for $f(RH)$ did not adequately describe the observed $f(RH)$, with low hygroscopic growth observed at RH values near 70%, in the OA dominated southeastern U.S. For the remainder of this analysis we will use the κ_{ext} parameterization (Eq. (6)) to extrapolate the extinction measured at the three discrete RH values to extinction at ambient RH. In the next section, we examine the relationship

Formatted: English (U.S.)

Formatted: Font color: Auto, English (U.S.)

Formatted: English (U.S.)

Formatted: English (U.S.)

Formatted: Font color: Auto, English (U.S.)

Formatted: English (U.S.)

Formatted: English (U.S.)

Formatted: English (U.S.), Superscript

Formatted: English (U.S.)

Formatted: English (U.S.), Superscript

Formatted: English (U.S.)

Formatted: Font: Font color: Auto, English (U.S.)

Formatted: Font: Font color: Auto, English (U.S.)

Formatted: Font: Font color: Auto, English (U.S.)

Formatted: English (U.S.)

Formatted: English (U.S.)

Formatted: English (U.S.)

Formatted: English (U.S.)

Formatted: English (U.S.)

Formatted: English (U.S.)

Formatted: Font: English (U.S.)

Formatted: Font: English (U.S.)

Formatted: English (U.S.)

Formatted: English (U.S.)

1 between κ_{ext} , determined from fitting the $f(RH)$ values (Eq. (6)) and κ_{chem} , calculated from particle composition
2 measurements (Eq. (2)). These parameters are related but not identical.

3 3.2 Relationship between κ_{chem} and κ_{ext}

4 Equations (2) and (6), which define κ_{chem} and κ_{ext} , are of similar form, but the $f(RH)$ term in Eq. (6) incorporates
5 aerosol extinction, which is a complex function of the particle size distribution and refractive index (Fig.
6 5 Wagner et al. (2015) present a method to generate a composite profile while maintaining distinction between
7 the mixed, transition, and free tropospheric layers. Composite profiles of the subset of 25 profiles that contained
8 valid $f(RH)$ data were generated by this technique (Fig. 4). As in the individual profile shown in Fig. 3, the
9 median dry extinction was a maximum in the well-mixed layer, declined through the transition layer, and was a
10 minimum in the free troposphere (Fig. 4a). The values of $f(RH)$, on the other hand, slightly increased with
11 altitude in the well-mixed and transition layers, and were a maximum in the free troposphere (Fig. 4b,c). Values
12 of $f(RH)$ were highly variable in the free troposphere, primarily because extinction values were low and signal
13 levels were noisy. The median inorganic fraction of PM1 increased from 0.35 ± 0.10 averaged over the well
14 mixed and transition layers to ~ 0.45 in the free troposphere. The organic aerosol in the well-mixed layer in
15 daytime was composed of aged secondary organic matter, primarily from biogenic sources (Kim et al., 2015; Xu
16 et al. 2015a,b). The measured mean values of $f(RH)$ for all layers was 1.43 ± 0.67 at $\sim 70\%$ RH and 2.28 ± 1.05 at
17 $\sim 90\%$ RH.

18 Using the method described in Fig. 1a and Sect. 2.3, the expected extinction at the dry, $\sim 70\%$, and $\sim 90\%$ RH
19 conditions was calculated. The $f(RH)$ values from these calculated extinctions are compared with the $f(RH)$
20 values from the CRDS measurements in Fig. 5. The calculated and measured $f(RH)$ are in excellent agreement
21 (slope=1.13, $r^2=0.81$) for the $\sim 90\%$ RH condition, but are less well correlated ($r^2=0.29$) for the $\sim 70\%$ RH
22 condition. This poorer correlation at the medium RH value may be associated with variability in organic
23 hygroscopicity, which dominates aerosol hygroscopicity at $RH < 80\%$. In section 3.3 we examine the range of
24 organic hygroscopicity that is consistent with our measurements within experimental uncertainty.

25). We use a size distribution and Mie scattering model to examine the relationship between κ_{chem} and κ_{ext} . The
26 aerosol was represented as a single mode lognormal size distribution with a fixed geometric standard deviation
27 of 1.5; the observed interdecile range for the data analyzed here was 1.42–1.60. The geometric mean diameter
28 was varied from 0.04 to 0.5 μm and the κ_{chem} value was varied from 0 to 1. The dry refractive index was fixed at
29 $1.53 + 0i$. At each geometric mean diameter and each value of κ_{chem} , the water uptake was determined at 10, 70,
30 and 90% RH, which approximately matched the measurement RH values for the low, medium and high CRDS
31 channels, and the extinction from the deliquesced size distribution was calculated. After determining the
32 extinction at all three RH levels, Eq. (6) was fitted to the calculated $f(RH)$ values to determine κ_{ext} . Thus the
33 chemically derived κ_{chem} could be compared with the optically derived κ_{ext} over a range of median particle
34 diameters and κ_{chem} values. As shown in Fig. 6, the ratio of $\kappa_{\text{ext}}/\kappa_{\text{chem}}$ varied from <0.4 to >2.0 over this range of
35 modal diameters and κ_{chem} values. However, for the range of κ_{chem} values of ~ 0.1 to ~ 0.4 and the geometric mean
36 diameter range from ~ 0.1 to ~ 0.2 , approximately matching the ranges observed in the southeastern U.S. (Corully
37 et al., 2015), the $\kappa_{\text{ext}}/\kappa_{\text{chem}}$ ratio generally lies between 0.6 and 1.0. Thus κ_{ext} and κ_{chem} are expected to be roughly

Formatted: English (U.S.)

Formatted: English (U.S.)

Formatted: English (U.S.)

~~equivalent in magnitude, with κ_{ext} tending toward smaller values, and to vary approximately proportionally (i.e., the value of $\kappa_{\text{ext}}/\kappa_{\text{chem}}$ does not change much with changing κ_{chem}).~~

~~The $\kappa_{\text{ext}}/\kappa_{\text{chem}}$ ratio from the simulation described above can be compared with the same ratio determined from the airborne extinction and aerosol composition measurements, also shown in Fig. 6. The measured mean $\kappa_{\text{ext}}/\kappa_{\text{chem}}$ was 0.52, with considerable dispersion. This ratio is lower than that expected from the simple single-mode lognormal model. This difference may arise because the atmospheric size distribution is not purely lognormal, and the magnitude of the modeled $\kappa_{\text{ext}}/\kappa_{\text{chem}}$ shown in Fig. 6 (i.e., the color scale) is sensitive to the assumed geometric standard deviation (although the overall shape of the pattern is not). Over the course of the measurements, κ_{ext} and κ_{chem} were correlated (Fig. 7). The relationships were more linear and with less dispersion for individual flights than for the dataset as a whole, suggesting day to day variability in mean size distribution, composition, and/or instrument performance. These data emphasize that κ_{ext} and κ_{chem} are related but substantially different parameters, coupled nonlinearly by Mie theory and the particle size distribution function, and cannot be substituted directly for one another.~~

~~3.3 Constraints on the hygroscopicity of OA~~

~~Organic aerosol matter dominated the composition of the submicron particles during both SENEX and SEAC⁴RS (e.g., Fig. 2a), averaging $65 \pm 10\%$ of the fine aerosol mass in the data analyzed here (Section 3.1). Published values for the hygroscopic growth parameter of OA, $\kappa_{\text{chem,OA}}$, vary widely between ~ 0 ~~← $\kappa_{\text{chem,OA}}$ ← and~~ 0.4 (e.g., Petters and Kreidenweis/Kreidenweis, 2007; Rickards et al., 2013; Suda et al., 2012). A parameterization linking $\kappa_{\text{chem,OA}}$ to the ratio of the oxidized OA fragment m/z 44 to total OA mass (f_{44}) as measured in the AMS has been developed (Duplissy et al., 2011). However, Rickards et al., (2013) find that this parameterization does not fit many available data, and that significant variations in aerosol chemical functionality, composition, and oxidation history affect $\kappa_{\text{chem,OA}}$. Cerully et al. (2015) show that, in the southeastern U. S., $\kappa_{\text{chem,OA}}$ is not simply related to oxidation state level, but to additional parameters including OA volatility. Values of κ_{chem} for atmospheric aerosols are commonly determined experimentally using measurements of droplet activation diameter in the supersaturated regime (e.g., Cerully et al., 2015; Chang et al. 2010; Dusek et al., 2010; Gunthe et al., 2009; Levin et al. 2012; Sihto et al., 2011) or using hygroscopic growth measurements in the subsaturated regime (Cappa et al., 2011; Cheung et al. 2015; Hersey et al., 2013; Malm et al., 2000; Mikhailov 2013; Nguyen et al., 2014; Sihto et al., 2011). Atmospheric variability in these measurements is compounded by potential measurement artifacts (Good et al., 2010b). Although not always explicitly calculated, the value of $\kappa_{\text{chem,OA}}$ often can be inferred from these studies. A review of results from the publications cited above suggests a range of mass-weighted total $\kappa_{\text{chem,OA}}$ from 0 to 0.2 ~~represents the organic hygroscopicity of the ambient aerosol well in a variety of environments, with best estimates of <0.1 for subsaturated measurements and >0.1 for supersaturated measurements. Consistent with these measurements, we use a fixed value of $\kappa_{\text{chem}}=0.085$ from Good et al., (2010a) for the water soluble fraction of OA, which approximately matches observed $f(RH)$ for our data. We further assume that the water soluble fraction of the total OA is 89%, based on measurements made at the Southern Oxidant and Aerosol Study (SOAS) surface site at Centreville, Alabama during the SENEX time frame (Washenfelder et al., 2015). The non-water soluble fraction is assumed to have $\kappa_{\text{chem}}=0$, yielding the mass-weighted $\kappa_{\text{chem,OA}}$ of 0.076 in Table 1 well represents the organic hygroscopicity of the ambient aerosol in a~~~~

Formatted: English (U.S.)

Formatted: English (U.S.)

Formatted: English (U.S.)

Formatted: Font: (Default) Times New Roman, English (U.S.)

Formatted: Heading 2

Formatted: Font: (Default) Times New Roman, English (U.S.)

Formatted: Font: Times New Roman, Not Bold, English (U.S.)

Formatted: English (U.S.)

Formatted: English (U.S.)

Formatted: English (U.S.)

Formatted: English (U.S.)

Formatted: English (U.S.)

Formatted: English (U.S.)

Formatted: English (U.S.)

1 variety of environments, with best estimates of <0.1 for subsaturated (hygroscopic growth) measurements and
2 >0.1 for supersaturated (CCN) measurements.

Formatted: English (U.S.)

3 It is possible that given the combined measurement uncertainties are sufficiently large that higher organic
4 fraction of the aerosol, the value of $\kappa_{chem,OA}$ is an important factor determining observed $f(RH)$. We can examine
5 which values of $\kappa_{chem,OA}$ might be consistent with our measurements. The relative within experimental
6 uncertainty to place constraints on this parameter. Some of the errors in the calculated extinction at the three RH
7 values ($\pm 34\%$, Section UHSAS sizing bias, UHSAS counting statistics, and UHSAS and AMS flow
8 uncertainties (Sect. 2.4)) are not independent and should cancel when calculating $f(RH)$. Ignoring these error
9 terms that cancel, relative errors in calculated $f(RH)_{70}$ of $\pm 7\%$ and in $f(RH)_{90}$ of $\pm 24\%$ were determined using the
10 Monte Carlo method described in Section 2.4. To calculate the range in $\kappa_{chem,OA}$ that was consistent with the
11 observed $f(RH)_{70}$ and $f(RH)_{90}$, the following approach was used: 1) For each measurement point, the inorganic
12 κ_{chem} determined from the AMS measurements was held constant. 2) A Monte Carlo simulation assigned a
13 random $\kappa_{chem,org}$ between 0.0 and 0.5, and the values of $f(RH)_{70}$ and $f(RH)_{90}$ were calculated. 3) When the
14 calculated $f(RH)_{70}$ and $f(RH)_{90}$ both agreed with the measured values within their uncertainties, the value of
15 $\kappa_{chem,OA}$ was recorded; otherwise step (2) was repeated. This process was repeated 50 times for each data point,
16 and the mean value of each $\kappa_{chem,OA}$ that was consistent with the data was recorded. Thus statistics were built for
17 the values of $\kappa_{chem,OA}$ that were consistent with observed hygroscopic growth at both the high and medium RH
18 conditions.

Formatted: English (U.S.)

Formatted: English (U.S.)

Formatted: English (U.S.)

Formatted: English (U.S.)

Formatted: English (U.S.)

Formatted: English (U.S.)

Formatted: Font: Bold, English (U.S.)

Formatted: English (U.S.)

Formatted: English (U.S.)

Formatted: English (U.S.)

19 A histogram of the values of mean $\kappa_{chem,OA}$ that were consistent with the $f(RH)$ observations within uncertainty
20 (Fig. 86) is heavily skewed toward zero, with the 50th, 75th, and 90th percentile values being 0.05, 0.10, and
21 0.17. This outcome demonstrates that a low value of $\kappa_{chem,OA}$ is necessary to match the observed $f(RH)$ values. In
22 particular, only with a best estimate of 0.05. Only values of $\kappa_{chem,OA} < 0.10$ can be consistent with the relatively
23 small increase in $f(RH)$ at the medium RH value of $\sim 70\%$ (Fig. 4a7a) in most (75%) of our data. Our analysis
24 assumes a homogeneous, size-independent internal mixture of the aerosol components, and does not account for
25 the possible presence of sparingly soluble OA compounds (Wex et al., 2009) or for the diameter dependence of
26 κ_{chem} (Good et al., 2010a). Nguyen et al. (2014, supplemental materials) suggest that κ_{chem} itself is a function of
27 RH due to an increasing osmotic coefficient with decreasing RH. In contrast, we find that a single, constant
28 κ_{chem} explains the $f(RH)$ at both 70% and 90% RH, but only if $\kappa_{chem,OA}$ is <0.10 for $>75\%$ of our data.

Formatted: English (U.S.)

Formatted: English (U.S.)

Formatted: English (U.S.)

Formatted: English (U.S.)

Formatted: English (U.S.)

Formatted: English (U.S.)

Formatted: English (U.S.)

Formatted: English (U.S.)

Formatted: English (U.S.)

Formatted: Font: Times New Roman, English (U.S.)

3.4 Parameterizing $f(RH)$

30 The hygroscopic growth of particles and $f(RH)$ can be calculated using the technique shown in Fig. 1a and Table
31 2 if discrete phase transitions can be ignored. However, a simplified parameterization based on optical
32 measurements alone (Fig. 1b) is useful when compositional or size distribution observations are not available, as
33 is often the case for in situ data from monitoring networks or measurements from mobile platforms. The often-
34 used γ parameterization (Eq. (1)) has the desired simplicity. In Fig. 7a we plot the observed $f(RH)$ found within
35 the well mixed layer in the single profile in Fig. 3. The γ parameterization with $RH_0=0$ did not match within
36 uncertainties the $f(RH)$ directly observed by the medium RH channel of the CRDS. This bias at $\sim 70\%$ RH
37 occurred frequently, as shown in the composite profiles (Fig. 4b) and in histogram form (Fig. 7c). The planetary
38 boundary layer in the southeastern US is often at humidities between 50 and 90% where the γ parameterization

Formatted: English (U.S.)

Formatted: English (U.S.)

could lead to overprediction of the ambient extinction by 20% or more. Because of these biases we have sought a different single-parameter representation of the $f(RH)$ curve.

In the Appendix, we use κ -Köhler and Mie theories to develop an alternative parameterization for $f(RH)$. This parameterization is given by

$$f(RH) \cong 1 + \kappa_{ext} \frac{RH}{100 - RH} \quad (6)$$

where κ_{ext} is the fitted parameter. When fitted to the three-point $f(RH)$ measurements in SENEX and SEAC⁴RS, both the κ_{ext} and γ parameterizations fit the high RH condition well (Figs. 4c, 7a). However, the κ_{ext} parameterization predicts the medium-RH extinction values better than does the γ parameterization for most of the data (Figs. 4b, 7a). In 17 of the 25 profiles for which valid hygroscopicity measurements were made, the κ_{ext} parameterization described the observed hygroscopic growth better than did the γ parameterization, as determined by a χ^2 statistic. This improved performance is shown Fig. 7c, where the fitted and measured $f(RH)$ values at the medium (70%) RH condition for the two parameterizations are compared. The ratio of fitted to measured $f(RH)$ values at 70% RH for κ_{ext} is centered near 1 and is symmetric, while that for γ is >1 for most of the data. Further, there are distinct differences in the fitted $f(RH)$ curves for the two approaches for $RH > 90\%$, with the κ_{ext} parameterization showing a more rapid increase in $f(RH)$ with increasing RH for these high humidity conditions (Fig. 7a). Preliminary evaluation of ambient atmospheric data acquired in February 2015 in Boulder, Colorado, US (Appendix) provides an example where the κ_{ext} curve more closely follows the observed $f(RH)$ for ambient particles at $RH > 90\%$ than does the γ parameterization. In the Supplemental Materials we also present additional analysis of data from the work of Zieger et al. (2013) that support the use of the κ_{ext} parameterization (Eq. (6)) in polluted and background continental cases where organic aerosol matter is likely to be a dominant component.

The γ parameterization (Eq. 1) is sometimes used with RH_0 set to some value other than 0, which is used here. In this application, $f(RH)$ is assumed to be zero for $RH < RH_0$, then increases sharply for $RH > RH_0$. That approach may produce a better fit to the measured $f(RH)$ values (e.g., Fig. 3a), but is probably most suitable for aerosols dominated by inorganic constituents which exhibit sharp deliquescence features. This approach is not appropriate for the continuous hygroscopic growth expected for the organic-dominated aerosols found in the southeastern US, and in particular for the deliquesced $f(RH)$ curve measured by the CRDS system.

In the Appendix we examine the relationship between κ_{ext} determined from fitting the $f(RH)$ values (Eq. (6)) and κ_{chem} calculated from particle composition measurements (Eq. (3)). These parameters are related but not identical.

3.5 Comparison of airborne and ground-based data

The airborne data can be compared with contemporaneous measurements at the SOAS ground site in Centreville of the change in σ_{ext} at wavelengths of 360–420 nm at two RH values (Attwood et al., 2014). Wagner et al. (2015) show that the airborne data measured in the well-mixed afternoon boundary layer ~~even near~~ the Centreville site agree well with the surface measurements. Attwood et al. (2014) fit the ground site data using the ~~gamma~~ parameterization (Eq. (1)) and find a decrease in hygroscopicity with increasing OA mass fraction that

Formatted: English (U.S.)

Formatted: English (U.S.)

Formatted: Font: (Default) Times New Roman, English (U.S.)

Formatted: Font: Times New Roman, Not Bold, English (U.S.)

Formatted: Heading 2

Formatted: English (U.S.)

Formatted: Font color: Auto, English (U.S.)

Formatted: English (U.S.)

Formatted: English (U.S.)

Formatted: English (U.S.)

1 is consistent with earlier studies in different aerosol types. Using the $f(RH)$ measurements by Attwood et al. and
2 solving Eq. (6), κ_{ext} can be calculated and compared with the airborne data. These values are plotted in Fig. 98
3 against the fraction of the total submicron non-refractory OA mass (note that this differs slightly from the F_{oa}
4 parameter reported by Attwood et al., 2014), as measured by a HR-TOF-AMS at the Centreville site (Xu et
5 al., 2015a,b). Also plotted are the values from the airborne data used in this analysis, restricted to AMS
6 mass concentrations $>8 \mu\text{g m}^{-3}$ to compare boundary layer air only. The airborne and ground data are similar,
7 with slopes of -0.24 ± 0.01 and -0.24 ± 0.04 , respectively (95% confidence intervals). The κ_{ext} values from the
8 ground site are higher; however, the κ_{ext} determined from a two-point $f(RH)$ measurement is particularly
9 sensitive to the accuracy of the RH measurements in the extinction cell, as shown by the dashed lines in Fig. 98,
10 which represent the variation in κ_{ext} due to the stated absolute uncertainty in the RH measurement at the ground
11 site of $\pm 3\%$. Extrapolating the central fits to an OA fraction of 1 yields a κ_{ext} of 0.030 for the airborne data and
12 0.067 for the data from the ground site. Recalling that the ratio of κ_{ext} to κ_{chem} is expected to be ~ 0.5 to 1 for
13 typical accumulation-mode size distributions (Fig. 6; Appendix), so a value of $\kappa_{chem,OA}$ of ~ 0.07 - 0.14 would be
14 expected at the SOAS ground site. These values are approximately generally consistent with the airborne results
15 showing a relatively low value of $\kappa_{chem,OA}$ (<0.10 for 75% of the data).

16 4.4 Discussion and Conclusions

17 ~~The submicron aerosol observed in typical summertime, fair weather, afternoon conditions in the southeastern~~
18 ~~U.S. was dominated by OA and displayed a modest increase in extinction with increasing humidity, $f(RH)$. The γ~~
19 ~~power-law parameterization, which is widely used to describe $f(RH)$ for atmospheric aerosols, did not effectively~~
20 ~~replicate the observations in this environment, primarily because actual hygroscopic growth was lower than~~
21 ~~parameterized growth at 70% RH. An alternative parameterization based on κ -Köhler theory that better describes~~
22 ~~the observed $f(RH)$ in the southeastern U.S. in summer was developed. This single-parameter κ_{ext} approximation~~
23 ~~is physically based, yet we caution that it also may not accurately describe $f(RH)$ in many circumstances. The~~
24 ~~submicron aerosol observed in typical summertime, fair-weather, afternoon conditions in the southeastern US~~
25 ~~displayed a vertical structure of a well-mixed layer between the surface and ~ 1100 m above the surface, a~~
26 ~~transition layer from ~ 1100 to ~ 2100 m, and the free troposphere above ~ 2100 m. Wagner et al. (2015) more~~
27 ~~fully describe this vertical structure and the gas-phase and aerosol characteristics of each layer, and show that~~
28 ~~ammonium and sulfate were the dominant inorganic aerosol constituents in all the layers. Within the well-mixed~~
29 ~~layer, the aerosol was $\sim 65\%$ OA, and declined to $\sim 50\%$ OA in the free troposphere. As a result of this~~
30 ~~composition, the aerosol on average was modestly hygroscopic, with $f(RH) = 1.43 \pm 0.67$ at $\sim 70\%$ RH and~~
31 ~~2.28 ± 1.05 at $\sim 90\%$ RH. Ammonium sulfate exhibits an $f(RH)$ of ~ 2 at $\sim 70\%$ RH (Langridge et al., 2011),~~
32 ~~attesting to the low hygroscopicity of the OA component.~~

33 ~~The hygroscopicity of OA varies with level of oxidation (O:C ratio), oxidation state, and solubility, among other~~
34 ~~parameters (e.g., Cappa et al., 2011; Cerully et al., 2015; Duplissy et al., 2011; Rickards et al., 2013). The large~~
35 ~~number of possible OA sources, oxidation histories, and compositions suggest a broad range of OA~~
36 ~~hygroscopicities. While the slope of the least-squares fit between the calculated and measured $f(RH)$ values at~~
37 ~~$\sim 70\%$ RH is 0.35, the r^2 value is only 0.43 and most of the data cluster near the 1:1 line; the low slope and poor~~

Formatted: English (U.S.)

Formatted: English (U.S.)

Formatted: English (U.S.)

Formatted: English (U.S.)

Formatted: English (U.S.)

Formatted: English (U.S.)

Formatted: English (U.S.)

Formatted: English (U.S.)

Formatted: English (U.S.)

Formatted: Heading 1, Space Before: 0 pt, After: 0 pt

Formatted: Font: (Default) Times New Roman, English (U.S.)

Formatted: Font: Times New Roman, Not Bold, English (U.S.)

1 correlation is driven by a small number of points. At ~90% RH, the calculated and measured $f(RH)$ are in
2 excellent agreement and are well correlated (Fig. 5b), probably because the well-characterized hygroscopicity of
3 the inorganic components is dominating the extinction at this higher RH level. This agreement at ~90% RH
4 precludes a high value of $\kappa_{chem,OA}$. For >75% of the data, a value of $\kappa_{chem,OA} < 0.1$ represents a reasonable upper
5 bound on subsaturated OA hygroscopicity in this environment.

6 ~~The value of $\kappa_{chem,OA} < 0.1$. For example, the abrupt phase transitions of inorganic salts sometimes observed in the
7 atmosphere (e.g., Santaripa et al., 2005) clearly cannot be described by this smooth function (nor by the γ
8 parameterization). More complex, multi-parameter descriptions of aerosol deliquescence and efflorescence (e.g.,
9 Kotchenruther et al., 1999; Mikhailov et al., 2013) are underconstrained by our three-point $f(RH)$ deliquescence
10 measurement. Further, the hygroscopic growth of aerosols dominated by larger particles, such as sea salt, dust,
11 and primary plant materials is unlikely to follow the κ_{ext} parameterization because the mid-visible extinction
12 efficiency for particles larger than 0.6 μm does not monotonically increase (Fig. 5). However, for a broad range
13 of typical aged continental aerosol size distributions and compositions ranging from background to moderately
14 polluted, from the boundary layer to the free troposphere, the κ_{ext} parameterization effectively describes the
15 $f(RH)$ curve for the deliquesced aerosol.~~

16 ~~By reconstructing the extinction based on independently measured composition and size distributions, the OA
17 was found to have had a κ Köhler hygroscopicity coefficient, $\kappa_{chem,org}$, that was < 0.10 for 75% of the data
18 assuming nearly all of the OA was water soluble. This value is broadly consistent most previous work measuring
19 atmospheric aerosol hygroscopicity in the subsaturated regime (Cheung et al. 2015; Hersey et al., 2013;
20 Mikhailov 2013; Nguyen et al., 2014; Sihto et al., 2011). Many chemistry-climate models use κ -Köhler theory to
21 predict the hygroscopic growth and ambient radiative properties of the aerosol (e.g., Liu et al., 2012). Because
22 OA is a substantial component of the aerosol in many environments (Zhang et al., 2007), it should be a priority
23 to use atmospheric measurements to continue to improve understanding of the factors that control OA
24 hygroscopicity and to evaluate the extent to which the findings reported here apply to other organic-rich
25 environments.~~

26 Finally, the γ power-law parameterization, which is widely used to describe $f(RH)$ for atmospheric aerosols, did
27 not effectively replicate many of the observations of $f(RH)$ in this environment, primarily because actual
28 hygroscopic growth was lower than parameterized growth at 70% RH. An alternative parameterization based on
29 κ -Köhler theory was developed and found to better describe the observed $f(RH)$ in the southeastern US in
30 summer. This κ_{ext} parameterization may be applicable to background and moderately polluted cases where the
31 extinction is dominated by organic particles with diameters $< 0.7 \mu\text{m}$.

32 Appendix

33 A.1 Derivation of the κ_{ext} parameterization

34 ~~The cube of the diameter growth factor gf_{diam} (Eq. (2)) is the volume growth factor. Relating the volume growth
35 factor to bulk $f(RH)$ however, involves the complicated variation of aerosol extinction efficiency as a function of
36 particle diameter, often described using Mie theory. As particles grow due to water uptake as RH increases, the~~

Formatted: English (U.S.)

Formatted: Font color: Auto, English (U.S.)

Formatted: English (U.S.)

Formatted: English (U.S.)

Formatted: English (U.S.)

Formatted: English (U.S.)

Formatted: English (U.S.)

1 extinction cross section can change non-linearly, and can even decrease (e.g., Bohren and Huffman, 1983).
2 However, as pointed out earlier (Chylek, 1978; Pinnick et al., 1980), for a physically realistic, polydisperse
3 aerosol composed of particles predominantly smaller than the wavelength of light (but larger than Rayleigh
4 scatterers), σ_{ext} is roughly proportional to integrated particle volume or mass. This proportionality results because
5 the extinction efficiency $a(D_p, n)$ for visible light can be approximated as a linear function of particle diameter
6 over the relatively broad size range of a polydisperse accumulation mode atmospheric aerosol (i.e., a is
7 proportional to D_p , Fig. A1). It then follows from Eq. (5) that $\sigma_{ext} \propto D_p^3$: extinction is proportional to volume.
8 Thus the relative change in extinction, $f(RH)$, is roughly proportional to the relative change in volume, which for
9 the case of a deliquescent aerosol is the volume growth factor gf_{vol} . The approximate proportionality between
10 extinction and volume is valid for particles smaller than the wavelength of light, which for these measurements
11 is 532 nm. The 10th to 90th percentile range for the geometric median diameters considered here was 120-170
12 nm, so this approximation is valid, even for particles at high RH. The approximate (no Kelvin effect) diameter
13 growth factor from κ -Köhler theory is given in Eq. (2). The cube of this this is then roughly proportional to gf_{vol}
14 and $f(RH)$:

$$15 \quad gf_{vol} \propto f(RH) \cong 1 + \kappa_{ext} \frac{RH}{100 - RH} \quad (A1)$$

16 where κ_{ext} is a dimensionless parameter fitted to observed $f(RH)$.

17 The volume-extinction approximate proportionality in Eq. (A1) applies for an aerosol of constant refractive
18 index, which is not the case for an atmospheric aerosol particle growing by addition of water with increasing RH
19 (Hänel, 1976; Hegg et al., 1993). The methodology to calculate ambient extinction (Section 2.3), which
20 incorporates the aerosol composition and size distribution measurements, can be used to estimate the effect of
21 aerosol water on the refractive index and its impact on extinction. Using this approach, the calculated mean
22 decrease in refractive index caused by condensed water reduces extinction by a factor of 0.81 ± 0.03 for the ~70%
23 RH channel and by 0.71 ± 0.03 for the ~90% RH channel. Because of this effect and the rough proportionality
24 between particle volume and extinction, Eq. A1 is only an approximation that should be used parametrically to
25 interpolate and extrapolate from discrete measurements on the $f(RH)$ curve. However, it is a physically based
26 representation of the expected functional form of $f(RH)$, unlike alternative parameterizations.

27 We caution that, like the γ parameterization, the κ_{ext} parameterization may not accurately describe $f(RH)$ in many
28 circumstances. For example, the abrupt phase transitions of inorganic salts sometimes observed in the
29 atmosphere (e.g., Santarpia et al., 2005) clearly cannot be described by this smooth function (nor by the γ
30 parameterization). More complex, multi-parameter descriptions of aerosol deliquescence and efflorescence (e.g.,
31 Kotchenruther et al., 1999; Mikhailov et al., 2013; Zieger et al., 2011) are underconstrained by our three-point
32 $f(RH)$ deliquescence measurement. Further, the hygroscopic growth of aerosols dominated by larger particles,
33 such as sea-salt, dust, and primary plant materials is unlikely to follow the κ_{ext} parameterization because the mid-
34 visible extinction efficiency for particles larger than 0.6 μm does not monotonically increase (Fig. A1).
35 However, for a broad range of typical aged continental aerosol size distributions and organic-rich compositions
36 ranging from background to moderately polluted, from the boundary layer to the free troposphere, the κ_{ext}
37 parameterization may effectively describe the $f(RH)$ curve for the deliquescent aerosol. Further examples from

Formatted: Font color: Auto, English (U.S.)

Formatted: English (U.S.)

Formatted: English (U.S.)

Formatted: Font color: Auto, English (U.S.)

Formatted: English (U.S.)

Formatted: English (U.S.), Superscript

Formatted: English (U.S.)

Formatted: English (U.S.), Superscript

Formatted: English (U.S.)

Formatted: Font: Font color: Auto, English (U.S.)

Formatted: Font: Font color: Auto, English (U.S.)

Formatted: Font: Font color: Auto, English (U.S.)

Formatted: English (U.S.)

Formatted: English (U.S.)

Formatted: English (U.S.)

Formatted: English (U.S.)

Formatted: English (U.S.)

Formatted: Font: English (U.S.)

Formatted: Font: English (U.S.)

Formatted: English (U.S.)

Formatted: Font color: Auto, English (U.S.)

Formatted: English (U.S.)

Formatted: English (U.S.)

1 the literature are presented in the Supplemental Materials, and Section A.3 provides additional data from
2 wintertime rooftop measurements supporting the use of the the κ_{ext} parameterization.

3 **A.2 Relationship between κ_{chem} and κ_{ext}**

4 Equations (2) and (A1), which define κ_{chem} and κ_{ext} , are of similar form, but the $f(RH)$ term in Eq. (A1)
5 incorporates aerosol extinction, which is a complex function of the particle size distribution and refractive index
6 (Fig. A1). We use a size distribution and Mie scattering model to examine the relationship between κ_{chem} and κ_{ext} .
7 The aerosol was represented as a single-mode lognormal size distribution with a fixed geometric standard
8 deviation of 1.5; the observed interdecile range for the data analyzed here was 1.42-1.60. The geometric mean
9 diameter was varied from 0.04 to 0.5 μm and the κ_{chem} value was varied from 0 to 1. The dry refractive index
10 was fixed at 1.53+0i. At each geometric mean diameter and each value of κ_{chem} , the water uptake was determined
11 at 10, 70, and 90% RH, which approximately matched the measurement RH values for the low, medium and
12 high CRDS channels, and the extinction from the deliquesced size distribution was calculated. After determining
13 the extinction at all three RH levels, Eq. (A1) was fitted to the calculated $f(RH)$ values to determine κ_{ext} . Thus the
14 chemically derived κ_{chem} could be compared with the optically derived κ_{ext} over a range of median particle
15 diameters and κ_{chem} values. As shown in Fig. A2, the ratio of $\kappa_{ext}/\kappa_{chem}$ varied from <0.4 to >2.0 over this range of
16 modal diameters and κ_{chem} values. However, for the range of κ_{chem} values of ~0.1 to ~0.4 and the geometric mean
17 diameter range from ~0.1 to ~0.2, approximately matching the ranges observed in the southeastern US (Ceruley
18 et al., 2015), the $\kappa_{ext}/\kappa_{chem}$ ratio generally lies between 0.6 and 1.0. Thus κ_{ext} and κ_{chem} are expected to be roughly
19 equivalent in magnitude, with κ_{ext} tending toward smaller values, and to vary approximately proportionally (i.e.,
20 the value of $\kappa_{ext}/\kappa_{chem}$ does not change much with changing κ_{chem}).

21 The $\kappa_{ext}/\kappa_{chem}$ ratio from the simulation described above can be compared with the same ratio determined from
22 the airborne extinction and aerosol composition measurements, also shown in Fig. A2. The measured mean
23 $\kappa_{ext}/\kappa_{chem}$ was 0.52, with considerable dispersion. This ratio is lower than that expected from the simple single-
24 mode lognormal model. This difference may arise because the atmospheric size distribution is not purely
25 lognormal, and the magnitude of the modeled $\kappa_{ext}/\kappa_{chem}$ shown in Fig. A2 (i.e., the color scale) is sensitive to the
26 assumed geometric standard deviation (although the overall shape of the pattern is not). Over the course of the
27 measurements, κ_{ext} and κ_{chem} were correlated (Fig. A3). The relationships were more linear and with less
28 dispersion for individual flights than for the dataset as a whole, suggesting day-to-day variability in mean size
29 distribution, composition, and/or instrument performance. These data emphasize that κ_{ext} and κ_{chem} are related but
30 substantially different parameters, coupled nonlinearly by Mie theory and the particle size distribution function,
31 and cannot be substituted directly for one another.

32 **—A.3. Additional data supporting use of the κ_{ext} parameterization**

33 The data presented in this manuscript show $f(RH)$ at only three RH values in the summertime, background
34 aerosol of the southeastern US. To provide evidence of the broader applicability of the κ_{ext} parameterization, in
35 this section we present additional measurements of $f(RH)$ obtained over a wide range of ambient RH values in a
36 different environment. Data were obtained from an open-path cavity ringdown spectrometer (OP-CRDS; Gordon

Formatted: English (U.S.)

Formatted: English (U.S.)

Formatted: English (U.S.)

Formatted: English (U.S.)

Formatted: English (U.S.)

Formatted: English (U.S.)

1 et al., 2015), which measured extinction at ambient conditions at a suburban rooftop site, the NOAA Earth
2 System Research Laboratory in Boulder, Colorado. The aircraft CRDS system was used to provide a dry
3 extinction value at $RH < 10\%$ for calculating $f(RH)$. An $f(RH)$ curve was obtained as the ambient RH varied due
4 to changing meteorological conditions. The same cTOF-AMS flown during SENEX measured simultaneously
5 and reported an aerosol that was $57 \pm 14\%$ organic, with ammonium nitrate and ammonium sulfate the dominant
6 inorganic species. Figure A3 shows $f(RH)$ for all periods when $\kappa_{chem} < 0.4$ during nearly continuous operation
7 from 2015/03/05 to 2015/06/04. These data are well fit by the κ_{ext} parameterization and less well by the γ
8 parameterization (Fig. A3). This $f(RH)$ curve extends from 11-97% RH and shows a sharp increase in $f(RH)$
9 above 80% RH that is well captured by the κ_{ext} functional form.

11 **Author contribution**

12 All authors contributed measurements and/or analyses for this manuscript. CB prepared the manuscript with
13 substantial contributions from ~~NAWNLW~~, TDG, JLJ, PC-J, RAW, AMM, and DMM.

15 **Acknowledgements**

16 This work was supported in part by NOAA's Health of the Atmosphere and Atmospheric Chemistry, Carbon
17 Cycle, and Climate Programs. PC-J, DAD, and JLJ were supported by NASA award
18 NNX12AC03G/NNX15AH33A and NSF award AGS-1243354. AGC was supported by NSF award AGS-
19 1242155. LX and NLN were supported by EPA award R834799 and NSF award AGS-1242258. This
20 publication's contents do not necessarily represent the official views of the respective granting agencies. The use
21 or mention of commercial products or services does not represent an endorsement by the authors or by any
22 agency.

23 **References**

Formatted: Font: (Default) Times New Roman, English (U.S.)

Formatted: Heading 1

Formatted: Font: Times New Roman, Not Bold, English (U.S.)

Formatted: English (U.S.)

Formatted: English (U.S.)

Formatted: English (U.S.), Superscript

Formatted: Font: (Default) Times New Roman, English (U.S.)

Formatted: Heading 1, Space Before: 0 pt, After: 0 pt

Formatted: Font: Times New Roman, Not Bold, English (U.S.)

Formatted: English (U.S.)

Formatted: Font: (Default) Times New Roman, English (U.S.)

Formatted: Heading 1, Space Before: 0 pt, After: 0 pt

Formatted: Font: Times New Roman, Not Bold, English (U.S.)

1 Attwood, A. R., Washenfelder, R. A., Brock, C. A., Hu, W., Baumann, K., Campuzano-Jost, P., Day, D. A.,
2 Edgerton, E. S., Murphy, D. M., Palm, B. B., McComiskey, A., Wagner, N. L., Sá, S. S., Ortega, A., Martin, S.
3 T., Jimenez, J. L. and Brown, S. S.: Trends in sulfate and organic aerosol mass in the Southeast U.S.: Impact on
4 aerosol optical depth and radiative forcing, *Geophys. Res. Lett.*, 41, 7701-7709, doi:10.1002/2014GL061669,
5 2014.

6 Bahreini, R., Dunlea, E. J., Matthew, B. M., Simons, C., Docherty, K. S., DeCarlo, P. F., Jimenez, J. L., Brock,
7 C. A. and Middlebrook, A. M.: Design and operation of a pressure-controlled inlet for airborne sampling
8 with an aerodynamic aerosol lens. *Aerosol Sci. Technol.*, 42, 465-471,
9 <http://doi.org/10.1080/02786820802178514>, 2008.

10 [Baron, P.: Aerosol Calculator Spreadsheet for Excel. Accessed 7 Dec. 2013 at](http://aerosols.wustl.edu/AAARworkshop08/software/AEROCALC-11-3-03.xls)
11 <http://aerosols.wustl.edu/AAARworkshop08/software/AEROCALC-11-3-03.xls>, 2001.

12 Bohren, C. F. and Huffman, D. R.: Absorption and Scattering of Light by Small Particles, John Wiley & Sons,
13 1983.

14 Boyd, C. M., Sanchez, J., Xu, L., Eugene, A. J., Nah, T., Tuet, W. Y., Guzman, M. I., and Ng, N. L.: Secondary
15 organic aerosol formation from the β -pinene+NO₃ system: effect of humidity and peroxy radical fate, *Atmos.*
16 *Chem. Phys.*, 15, 7497-7522, doi:10.5194/acp-15-7497-2015, 2015.

17 Brock, C. A., Cozic, J., Bahreini, R., Froyd, K. D., Middlebrook, A. M., McComiskey, A., Brioude, J., Cooper,
18 O. R., Stohl, A., Aikin, K. C., de Gouw, J. A., Fahey, D. W., Ferrare, R. A., Gao, R. S., Gore, W., Holloway, J.
19 S., Hübler, G., Jefferson, A., Lack, D. A., Lance, S., Moore, R. H., Murphy, D. M., Nenes, A., Novelli, P. C.,
20 Nowak, J. B., Ogren, J. A., Peischl, J., Pierce, R. B., Pilewskie, P., Quinn, P. K., Ryerson, T. B., Schmidt, K. S.,
21 Schwarz, J. P., Sodemann, H., Spackman, J. R., Stark, H., Thomson, D. S., Thornberry, T., Veres, P., Watts, L.
22 A., Warneke, C. and Wollny, A. G.: Characteristics, sources, and transport of aerosols measured in spring 2008
23 during the aerosol, radiation, and cloud processes affecting Arctic Climate (ARCPAC) Project, *Atmos. Chem.*
24 *Phys.*, 11, 2423-2453, doi:10.5194/acp-11-2423-2011, 2011.

25 Brock, C. A., Wagner, N. L., Anderson, B. E., Beyersdorf, A., Campuzano-Jost, P., Day, D. A., Diskin, G. S.,
26 Gordon, T. D., Jimenez, J. L., Lack, D. L., Liao, J., Middlebrook, A. M.¹, Richardson, M. S., Welti, A., Ziemba,
27 L. D., and Murphy, D. M.: Aerosol optical properties in the southeastern United States in summer--Part 2:
28 Sensitivity of aerosol optical depth to meteorological and aerosol parameters, submitted to *Atmos. Chem. Phys.*
29 *Disc.*, 2015.

30 Cai, Y., Montague, D. and Mooiweer-Bryan, W.: Performance characteristics of the ultra high sensitivity aerosol
31 spectrometer for particles between 55 and 800 nm: Laboratory and field studies, *J. Aerosol Sci.*, 39, 759-769,
32 doi:10.1016/j.jaerosci.2008.04.007, 2008.

33 Canagaratna, M., Jayne, J., Jimenez, J., Allan, J., Alfarra, M., Zhang, Q., Onasch, T. B., Drewnick, F., Coe, H.,
34 Middlebrook, A. M., Delia, A., Williams, L. R., Trimborn, A. M., Northway, M. J., DeCarlo, P. F., Kolb, C. E.,
35 Davidovits, P., Worsnop, D. R.: Chemical and microphysical characterization of ambient aerosols with the
36 aerodyne aerosol mass spectrometer, *Mass Spec. Rev.*, 26, 185-222, 2007.

23

Brock et al. Aerosol Hygroscopicity in the Southeastern [U.S.](#)

Formatted: English (U.S.)

Formatted: Widow/Orphan control, Adjust space between Latin and Asian text, Adjust space between Asian text and numbers, Tab stops: Not at 0.99 cm + 1.98 cm + 2.96 cm + 3.95 cm + 4.94 cm + 5.93 cm + 6.91 cm + 7.9 cm + 8.89 cm + 9.88 cm + 10.86 cm + 11.85 cm

Formatted: Width: 20.99 cm, Height: 29.66 cm

Formatted: Widow/Orphan control, Adjust space between Latin and Asian text, Adjust space between Asian text and numbers, Tab stops: Not at 0.99 cm + 1.98 cm + 2.96 cm + 3.95 cm + 4.94 cm + 5.93 cm + 6.91 cm + 7.9 cm + 8.89 cm + 9.88 cm + 10.86 cm + 11.85 cm

Formatted: Position: Horizontal: Left, Relative to: Column, Vertical: In line, Relative to: Margin, Wrap Around

1 [Cappa, C. D., Che, D. L., Kessler, S. H., Kroll, J. H. and Wilson, K. L.: Variations in organic aerosol optical and](#)
2 [hygroscopic properties upon heterogeneous OH oxidation, *J. Geophys. Res.*, 116, D15204,](#)
3 [doi:10.1029/2011JD015918, 2011.](#)

4 [Carrico, C. M., Kreidenweis, S. M., Malm, W. C., Day, D. E., Lee, T., Carrillo, J., McMeeking, G. R. and](#)
5 [Collett Jr., J. L.: Hygroscopic growth behavior of a carbon-dominated aerosol in Yosemite National Park,](#)
6 [Atmos. Environ., 39, 1393–1404, doi:10.1016/j.atmosenv.2004.11.029, 2005.](#)

7 Cerully, K. M., Bougiatioti, A., Hite Jr., J. R., Guo, H., Xu, L., Ng, N. L., Weber, R., and Nenes, A.: On the link
8 between hygroscopicity, volatility, and oxidation state of ambient and water-soluble aerosols in the southeastern
9 United States, *Atmos. Chem. Phys.*, 15, 8679–8694, doi:10.5194/acp-15-8679-2015, 2015.

10 Chang, R. Y.-W., Slowik, J. G., Shantz, N. C., Vlasenko, A., Liggio, J., Sjostedt, S. J., Leaitch, W. R. and
11 Abbatt, J. P. D.: The hygroscopicity parameter (κ) of ambient organic aerosol at a field site subject to biogenic
12 and anthropogenic influences: relationship to degree of aerosol oxidation, *Atmos. Chem. Phys.*, 10, 5047–5064,
13 doi:10.5194/acp-10-5047-2010, 2010.

14 Charlson, R. J., Horvath, H. and Poeschel, R. F.: The direct measurement of atmospheric light scattering
15 coefficient for studies of visibility and pollution, *Atmos. Environ.* 1, 469-478, 1967.

16 Cheung, H. H. Y., Yeung, M. C., Li, Y. J., Lee, B. P. and Chan, C. K.: Relative humidity-dependent HTDMA
17 measurements of ambient aerosols at the HKUST supersite in Hong Kong, China, *Aerosol. Sci. Technol.*, 49,
18 643–654, doi:10.1080/02786826.2015.1058482, 2015.

19 Chylek, P.: Extinction and liquid water content of fogs and clouds, *J. Atmos. Sci.*, 35, 296–300, 1978.

20 Covert, D. S. and Charlson, R. J.: A study of the relationship of chemical composition and humidity to light
21 scattering by aerosols, *J. Appl. Meteor.*, 11, 968-976, 1972.

22 [Crumeyrolle, S., Chen, G., Ziemba, L., Beyersdorf, A., Thornhill, L., Winstead, E., Moore, R. H., Shook, M. A.,](#)
23 [Hudgins, C. and Anderson, B. E.: Factors that influence surface PM_{2.5} values inferred from satellite](#)
24 [observations: perspective gained for the U.S. Baltimore–Washington metropolitan area during DISCOVER-AQ,](#)
25 [Atmos. Chem. Phys., 14, 2139–2153, doi:10.5194/acp-14-2139-2014, 2014.](#)

26 Day, D. A., Campuzano-Jost, P., Palm, B. B.,^{1,2} Hu, W., Nault, B. A., Wooldridge, P. J., Cohen, R. C.,
27 Docherty, K. S., Wagner, N. L., Jimenez, J. L.: Observations of particle organic nitrate from airborne and ground
28 platforms in North America: Insights into vertical and geographical distributions, gas/particle partitioning,
29 losses, and contributions to total particle nitrate, manuscript in preparation, 2015.

30 DeCarlo, P. F., Kimmel, J. R., Trimborn, A., Northway, M. J., Jayne, J. T., Aiken, A. C., Gonin, M., Fuhrer, K.,
31 Horvath, T., Docherty, K. S., Worsnop, D. R. and Jimenez, J. L.: Field-deployable, high-resolution, time-of-
32 flight aerosol mass spectrometer, *Anal. Chem.*, 78, 8281–8289, doi:10.1021/ac061249n, 2006.

33 Doherty, S. J. P. K. Quinn, A. Jefferson, C. M. Carrico, T. L. Anderson, and D. Hegg.: A comparison and
34 summary of aerosol optical properties as observed in situ from aircraft, ship, and land during ACE-Asia, *J.*
35 *Geophys. Res.*, 110, D04201, doi:10.1029/2004JD004964, 2005.

24

Brock et al. Aerosol Hygroscopicity in the Southeastern [U.S.](#)^{US}

Formatted: Widow/Orphan control,
Adjust space between Latin and Asian
text, Adjust space between Asian text
and numbers, Tab stops: Not at 0.99
cm + 1.98 cm + 2.96 cm + 3.95 cm
+ 4.94 cm + 5.93 cm + 6.91 cm +
7.9 cm + 8.89 cm + 9.88 cm +
10.86 cm + 11.85 cm

Formatted: Widow/Orphan control,
Adjust space between Latin and Asian
text, Adjust space between Asian text
and numbers, Tab stops: Not at 0.99
cm + 1.98 cm + 2.96 cm + 3.95 cm
+ 4.94 cm + 5.93 cm + 6.91 cm +
7.9 cm + 8.89 cm + 9.88 cm +
10.86 cm + 11.85 cm

Formatted: Position: Horizontal: Left,
Relative to: Column, Vertical: In line,
Relative to: Margin, Wrap Around

1 Draper, D. C., Farmer, D. K., Desyaterik, Y. and Fry, J. L.: A comparison of secondary organic aerosol (SOA)
2 yields and composition from ozonolysis of monoterpenes at varying concentrations of NO₂, Atmos. Chem. Phys.
3 Disc., 15, 14923–14960, doi:10.5194/acpd-15-14923-2015, 2015.

4 Dunlea, E. J., DeCarlo, P. F., Aiken, A. C., Kimmel, J. R., Peltier, R. E., Weber, R. J., Tomlinson, J.,
5 Collins, D. R., Shinozuka, Y., McNaughton, C. S., Howell, S. G., Clarke, A. D., Emmons, L. K., Apel, E. C.,
6 Pfister, G. G., van Donkelaar, A., Martin, R. V., Millet, D. B., Heald, C. L., and Jimenez, J. L.: Evolution of
7 Asian aerosols during transpacific transport in INTEX-B, Atmos. Chem. Phys., 9, 7257-7287, doi:10.5194/acp-
8 9-7257-2009, 2009.

9 Duplissy, J., DeCarlo, P. F., Dommen, J., Alfarra, M. R., Metzger, A., Barmapadimos, I., Prevot, A. S. H.,
10 Weingartner, E., Tritscher, T., Gysel, M., Aiken, A. C., Jimenez, J. L., Canagaratna, M. R., Worsnop, D. R.,
11 Collins, D. R., Tomlinson, J. and Baltensperger, U.: Relating hygroscopicity and composition of organic aerosol
12 particulate matter, Atmos. Chem. Phys., 11, 1155–1165, doi:10.5194/acp-11-1155-2011, 2011.

13 Dusek, U., Frank, G. P., Curtius, J., Drewnick, F., Schneider, J., Kürten, A., Rose, D., Andreae, M. O.,
14 Borrmann, S. and Pöschl, U.: Enhanced organic mass fraction and decreased hygroscopicity of cloud
15 condensation nuclei (CCN) during new particle formation events, Geophys. Res. Lett., 37, L03804,
16 doi:10.1029/2009GL040930, 2010.

17 ~~Friedlander, S. K. and Wang, C.S.: The self-preserving particle size distribution for coagulation by Brownian~~
18 ~~motion, J. Colloid Interface Sci., 22, 2, 126-132, doi:/10.1016/0021-9797(66)90073-7, 1966.~~

19 Esteve, A. R., Ogren, J. A., Sheridan, P. J., Andrews, E., Holben, B. N., and Utrillas, M. P.: Sources of
20 discrepancy between aerosol optical depth obtained from AERONET and in-situ aircraft profiles, Atmos. Chem.
21 Phys., 12, 2987-3003, doi:10.5194/acp-12-2987-2012, 2012.

22 Ferrare, R., Melfi, S., Whiteman, D., Evans, K. and Leifer, R.: Raman lidar measurements of aerosol extinction
23 and backscattering I. Methods and comparisons, J. Geophys. Res., 103, 19663-19672, doi:10.1029/98JD01646,
24 1998.

25 Fry, J. L., Kiendler-Scharr, A., Rollins, A. W., Wooldridge, P. J., Brown, S. S., Fuchs, H., Dubé, W., Mensah,
26 A., dal Maso, M., Tillmann, R., Dorn, H.-P., Brauers, T., and Cohen, R. C.: Organic nitrate and secondary
27 organic aerosol yield from NO₃- oxidation of α-pinene evaluated using a gas-phase kinetics/aerosol partitioning
28 model, Atmos. Chem. Phys., 9, 1431–1449, doi:10.5194/acp-9-1431-2009, 2009.

29 Good, N., Topping, D. O., Allan, J. D., Flynn, M., Fuentes, E., Irwin, M., Williams, P. I., Coe, H. and
30 McFiggans, G.: Consistency between parameterisations of aerosol hygroscopicity and CCN activity during the
31 RHaMBLe discovery cruise, Atmos. Chem. Phys., 10, 3189–3203, 2010a.

32 Good, N., Topping, D. O., Duplissy, J., Gysel, M., Meyer, N. K., Metzger, A., Turner, S. F., Baltensperger, U.,
33 Ristovski, Z., Weingartner, E., Coe, H., and McFiggans, G.: Widening the gap between measurement and
34 modelling of secondary organic aerosol properties? Atmos. Chem. Phys., 10, 2577–2593, 2010b.

Formatted: Widow/Orphan control, Adjust space between Latin and Asian text, Adjust space between Latin and Asian text and numbers, Tab stops: Not at 0.99 cm + 1.98 cm + 2.96 cm + 3.95 cm + 4.94 cm + 5.93 cm + 6.91 cm + 7.9 cm + 8.89 cm + 9.88 cm + 10.86 cm + 11.85 cm

Formatted: Position: Horizontal: Left, Relative to: Column, Vertical: In line, Relative to: Margin, Wrap Around

1 [Gordon, T. D., Wagner, N. L., Richardson, M. S., Law, D. C., Wolfe, D., Eloranta, E. W., Brock, C. A., Erdesz,](#)
2 [F. and Murphy, D. M.: Design of a novel open-path aerosol extinction cavity ringdown spectrometer, *Aerosol*](#)
3 [Science and Technology, 49, 717-726, doi:10.1080/02786826.2015.1066753, 2015.](#)

4 Gunthe, S. S., King, S. M., Rose, D., Chen, Q., Roldin, P., Farmer, D. K., Jimenez, J. L., Artaxo, P., Andreae, M.
5 O., Martin, S. T. and Pöschl, U.: Cloud condensation nuclei in pristine tropical rainforest air of Amazonia: size-
6 resolved measurements and modeling of atmospheric aerosol composition and CCN activity, *Atmos. Chem.*
7 *Phys.*, 9, 7551–7575, doi:10.5194/acp-9-7551-2009, 2009.

8 [Guo, H., Xu, L., Bougiatioti, A., Cerully, K. M., Capps, S. L., Hite Jr., J. R., Carlton, A. G., Lee, S.-H., Bergin,](#)
9 [M. H., Ng, N. L., Nenes, A., and Weber, R. J.: Fine-particle water and pH in the southeastern United States,](#)
10 [Atmos. Chem. Phys., 15, 5211–5228, doi:10.5194/acp-15-5211-2015, 2015.](#)

11 Hale, G. M. and Querry, M. R.: Optical constants of water in the 200-nm to 200- μ m wavelength region, *Appl.*
12 *Opt.*, 12, 555–563, 1973.

13 Hand, J. L. and Kreidenweis, S. M.: A new method for retrieving particle refractive index and effective density
14 from aerosol size distribution data, *Aerosol. Sci. Tech.*, 36, 1012-1026, doi:10.1080/02786820290092276, 2002.

15 Hänel, G.: Computation of the extinction of visible radiation by atmospheric aerosol particles as a function of the
16 relative humidity, based upon measured properties, *J. Aerosol Sci.*, 3, 377-386, doi:
17 [http://dx.doi.org/10.1016/0021-8502\(72\)90092-4](http://dx.doi.org/10.1016/0021-8502(72)90092-4), 1972a.

18 Hänel, G.: The ratio of the extinction coefficient to the mass of atmospheric aerosol particles as a function of the
19 relative humidity, *J. Aerosol Sci.*, 3, 455-460, doi: [http://dx.doi.org/10.1016/0021-8502\(72\)90075-4](http://dx.doi.org/10.1016/0021-8502(72)90075-4), 1972b.

20 Hänel, G.: Single-scattering albedo of atmospheric aerosol particles as a function of relative humidity, *J. Atmos.*
21 *Sci.*, 33, 1120-1124, 1976.

22 Haynes, W. M., Lide, D. R. and Bruno, T. J.: CRC handbook of chemistry and physics : a ready-reference book
23 of chemical and physical data, CRC Press, Boca Raton, FL, [U.S.,USA](#), 2014.

24 Hegg, D., Larson, T. and Yuen, P. F.: A theoretical study of the effect of relative humidity on light scattering by
25 tropospheric aerosols, *J. Geophys. Res.*, 98, 18435–18439, 1993.

26 Hersey, S. P., Craven, J. S., Metcalf, A. R., Lin, J., Latham, T., Suski, K. J., Cahill, J. F., Duong, H. T.,
27 Sorooshian, A., Jonsson, H. H., Shiraiwa, M., Zuend, A., Nenes, A., Prather, K. A., Flagan, R. C. and Seinfeld,
28 J. H.: Composition and hygroscopicity of the Los Angeles Aerosol: CalNex, *J. Geophys. Res.*, 118, 3016–3036,
29 doi:10.1002/jgrd.50307, 2013.

30 Hodas, N., Zuend, A., Mui, W., Flagan, R. C. and Seinfeld, J. H.: Influence of particle phase state on the
31 hygroscopic behavior of mixed organic–inorganic aerosols, *Atmos. Chem. Phys.*, 15, 5027-5045,
32 doi:10.5194/acp-15-5027-2015, 2015.

33 IPCC [Stocker, T. F., Qin, D., Plattner, G.-K., Tignor, M., Allen, S. K., Boschung, J., Nauels, A., Xia, Y., Bex,
34 V. and Midgley, P. M. (Eds.)]: Climate Change 2013: The Physical Science Basis. Contribution of Working

26

Brock et al. Aerosol Hygroscopicity in the Southeastern [U.S.,US](#)

Formatted: Widow/Orphan control, Adjust space between Latin and Asian text, Adjust space between Asian text and numbers, Tab stops: Not at 0.99 cm + 1.98 cm + 2.96 cm + 3.95 cm + 4.94 cm + 5.93 cm + 6.91 cm + 7.9 cm + 8.89 cm + 9.88 cm + 10.86 cm + 11.85 cm

Formatted: Widow/Orphan control, Adjust space between Latin and Asian text, Adjust space between Asian text and numbers, Tab stops: Not at 0.99 cm + 1.98 cm + 2.96 cm + 3.95 cm + 4.94 cm + 5.93 cm + 6.91 cm + 7.9 cm + 8.89 cm + 9.88 cm + 10.86 cm + 11.85 cm

Formatted: Position: Horizontal: Left, Relative to: Column, Vertical: In line, Relative to: Margin, Wrap Around

1 Group I to the Fifth Assessment Report of the Intergovernmental Panel on Climate Change. Cambridge
2 University Press, Cambridge, United Kingdom and New York, NY, USA, doi:10.1017/CBO9781107415324,
3 2013.

4 [Kahn, R. A.: Reducing the uncertainties in direct aerosol radiative forcing, *Surv. Geophys.*, **33**, 701–721,](#)
5 [doi:10.1007/s10712-011-9153-z, 2011.](#)

6 Kasten, F.: Visibility forecast in the phase of pre-condensation, *Tellus*, **21**, 631st in the p

7 [Kim, P. S., Jacob, D. J., Fisher, J. A., Travis, K., Yu, K., Zhu, L., Yantosca, R. M., Sulprizio, M. P., Jimenez, J.](#)
8 [L., Campuzano-Jost, P., Froyd, K. D., Liao, J., Hair, J. W., Fenn, M. A., Butler, C. F., Wagner, N. L., Gordon, T.](#)
9 [D., Welti, A., Wennberg, P. O., Crouse, J. D., St. Clair, J. M., Teng, A. P., Millet, D. B., Schwarz, J. P.,](#)
10 [Markovic, M. Z., and Perring, A. E.: Sources, seasonality, and trends of southeast US aerosol: an integrated](#)
11 [analysis of surface, aircraft, and satellite observations with the GEOS-Chem chemical transport model, *Atmos.*](#)
12 [Chem. Phys.](#), **15**, 10411–10433, doi:10.5194/acp-15-10411-2015, 2015.

13 [Koloutsou-Vakakis, S., Rood, M. J., Nenes, A. and Pilinis, C.: Modeling of aerosol properties related to direct](#)
14 [climate forcing, *J. Geophys. Res.*, **103**, 17009–17032, 1998.](#)

15 Kotchenruther, R. A., Hobbs, P. V. and Hegg, D. A.: Humidification factors for atmospheric aerosols off the
16 mid-Atlantic coast of the United States, *J. Geophys. Res.*, **104**, 2239–2251, 1999.

17 Langridge, J. M., Richardson, M. S., Lack, D., Law, D. and Murphy, D. M.: Aircraft instrument for
18 comprehensive characterization of aerosol optical properties, Part I: Wavelength-dependent optical extinction
19 and its relative humidity dependence measured using cavity ringdown spectroscopy, *Aerosol Sci. Tech.*, **45**,
20 1305–1318, doi:10.1080/02786826.2011.592745, 2011.

21 Levin, E. J. T., Prenni, A. J., Petters, M. D., Kreidenweis, S. M., Sullivan, R. C., Atwood, S. A., Ortega, J.,
22 DeMott, P. J. and Smith, J. N.: An annual cycle of size-resolved aerosol hygroscopicity at a forested site in
23 Colorado, *J. Geophys. Res.*, **117**, D06201, doi:10.1029/2011JD016854, 2012.

24 Liao, J., Froyd, K. D., Murphy, D. M., Keutsch, F. N., Yu, G., Wennberg, P. O., St. Clair, J. M., Crouse, J. D.,
25 Wisthaler, A., Mikoviny, T., Jimenez, J. L., Campuzano-Jost, P., Day, D. A., Hu, W., Ryerson, T. B., Pollack, I.
26 B., Peischl, J., Anderson, B. E., Ziemba, L. D., Blake, D. R., Meinardi, S. and Diskin, G.: Airborne
27 measurements of organosulfates over the continental U.S., *J. Geophys. Res.*, **120**, 2990–3005,
28 doi:10.1002/2014JD022378, 2015.

29 Liu, X., Easter, R. C., Ghan, S. J., Zaveri, R., Rasch, P., Shi, X., Lamarque, J. F., Gettelman, A., Morrison, H.,
30 Vitt, F., Conley, A., Park, S., Neale, R., Hannay, C., Ekman, A. M. L., Hess, P., Mahowald, N., Collins, W.,
31 Iacono, M. J., Bretherton, C. S., Flanner, M. G. and Mitchell, D.: Toward a minimal representation of aerosols in
32 climate models: description and evaluation in the Community Atmosphere Model CAM5, *Geosci. Model Dev.*,
33 **5**, 709–739, doi:10.5194/gmd-5-709-2012, 2012.

Formatted: Widow/Orphan control,
Adjust space between Latin and Asian
text, Adjust space between Asian text
and numbers, Tab stops: Not at 0.99
cm + 1.98 cm + 2.96 cm + 3.95 cm +
4.94 cm + 5.93 cm + 6.91 cm +
7.9 cm + 8.89 cm + 9.88 cm +
10.86 cm + 11.85 cm

Formatted: Widow/Orphan control,
Adjust space between Latin and Asian
text, Adjust space between Asian text
and numbers, Tab stops: Not at 0.99
cm + 1.98 cm + 2.96 cm + 3.95 cm +
4.94 cm + 5.93 cm + 6.91 cm +
7.9 cm + 8.89 cm + 9.88 cm +
10.86 cm + 11.85 cm

Formatted: Position: Horizontal: Left,
Relative to: Column, Vertical: In line,
Relative to: Margin, Wrap Around

1 Malm, W. C., Day, D. E. and Kreidenweis, S. M.: Light scattering characteristics of aerosols as a function of
2 relative humidity: Part I—A comparison of measured scattering and aerosol concentrations using the theoretical
3 models, *J. Air Waste Mgmt. Assoc.*, 50, 686-700, doi: 10.1080/10473289.2000.10464117, 2000.

4 Massoli, P., Bates, T., Quinn, P. and Lack, D.: Aerosol optical and hygroscopic properties during TexAQS-
5 GoMACCS 2006 and their impact on aerosol direct radiative forcing, *J. Geophys. Res.*, 114,
6 D00F07,doi:10.1029/2008JD011604, 2009.

7 [McNaughton, C. S., Clarke, A. D., Howell, S. G., Pinkerton, M., Anderson, B., Thornhill, L., Hudgins, C.,
8 Winstead, E., Dibb, J. E., Scheuer, E. and Maring, H.: Results from the DC-8 Inlet Characterization Experiment
9 \(DICE\): Airborne versus surface sampling of mineral dust and sea salt aerosols, *Aerosol Sci. Technol.*, 41, 136-
10 159, doi: 10.1080/02786820601118406, 2007.](#)

11 Middlebrook, A. M., Bahreini, R., Jimenez, J. L. and Canagaratna, M. R.: Evaluation of composition-dependent
12 collection efficiencies for the Aerodyne aerosol mass spectrometer using field data, *Aerosol Sci. Tech.*, 46, 258–
13 271, doi:10.1080/02786826.2011.620041, 2012.

14 Mikhailov, E., Vlasenko, S., Rose, D. and Pöschl, U.: Mass-based hygroscopicity parameter interaction model
15 and measurement of atmospheric aerosol water uptake, *Atmos. Chem. Phys.*, 13, 717–740, doi:10.5194/acp-13-
16 717-2013, 2013.

17 [Murphy, D. M.: The effects of molecular weight and thermal decomposition on the sensitivity of a thermal
18 desorption aerosol mass spectrometer, *Aerosol Sci. Technol.*, 50, 118-125,
19 doi:10.1080/02786826.2015.1136403, 2016.](#)

20 [Nemesure, S., Wagener, R. and Schwartz, S. E.: Direct shortwave forcing of climate by the anthropogenic
21 sulfate aerosol: Sensitivity to particle size, composition, and relative humidity, *J. Geophys. Res.*, 100,
22 26105,26116, 1995.](#)

23 Nguyen, T. K. V., Petters, M. D., Suda, S. R., Guo, H., Weber, R. J. and Carlton, A. G.: Trends in particle-phase
24 liquid water during the Southern Oxidant and Aerosol Study, *Atmos. Chem. Phys.*, 14, 10911–10930,
25 doi:10.5194/acp-14-10911-2014, 2014.

26 Petters, M. D. and Kreidenweis, S. M.: A single parameter representation of hygroscopic growth and cloud
27 condensation nucleus activity, *Atmos. Chem. Phys.*, 7, 1961-1971, 2007.

28 Petzold, A., Formenti, P., Baumgardner, D., Bundke, U., Coe, H., Curtius, J., DeMott, P. J., Flagan, R. C.,
29 Fiebig, M., Hudson, J. G., McQuaid, J., Minikin, A., Roberts, G. C., and Wang, J.: In situ measurements of
30 aerosol particles, in: *Airborne Measurements for Environmental Research: Methods and Instruments*, J. Wiley &
31 Sons, ISBN: 978-3-527-40996-9, 157-224, 2013.

32 Pilat, M. J. and Charlson, R. J.: Theoretical and optical studies of humidity effects on the size distribution of a
33 hygroscopic aerosol, *J. Rech. Atmos.*, 165-170, 1966.

34 Pinnick, R. G., Jennings, S. G. and Chýlek, P.: Relationships between extinction, absorption, backscattering, and
35 mass content of sulfuric acid aerosols, *J. Geophys. Res.*, 85, 4059–4066, 1980.

28
Brock et al. Aerosol Hygroscopicity in the Southeastern [U.S.-US](#)

Formatted: Widow/Orphan control, Adjust space between Latin and Asian text, Adjust space between Asian text and numbers, Tab stops: Not at 0.99 cm + 1.98 cm + 2.96 cm + 3.95 cm + 4.94 cm + 5.93 cm + 6.91 cm + 7.9 cm + 8.89 cm + 9.88 cm + 10.86 cm + 11.85 cm

Formatted: Widow/Orphan control, Adjust space between Latin and Asian text, Adjust space between Asian text and numbers, Tab stops: Not at 0.99 cm + 1.98 cm + 2.96 cm + 3.95 cm + 4.94 cm + 5.93 cm + 6.91 cm + 7.9 cm + 8.89 cm + 9.88 cm + 10.86 cm + 11.85 cm

Formatted: Position: Horizontal: Left, Relative to: Column, Vertical: In line, Relative to: Margin, Wrap Around

1 Pringle, K. J., Tost, H., Pozzer, A., Pöschl, U. and Lelieveld, J.: Global distribution of the effective aerosol
2 hygroscopicity parameter for CCN activation, *Atmos. Chem. Phys.*, 10, 5241–5255, doi:10.5194/acp-10-5241-
3 2010, 2010.

4 Quinn, P. K., Bates, T. S., Baynard, T., Clarke, A. D., Onasch, T. B., Wang, W., Rood, M. J., Andrews, E.,
5 Allan, J., Carrico, C. M., Coffman, D. and Worsnop, D.: Impact of particulate organic matter on the relative
6 humidity dependence of light scattering: A simplified parameterization, *Geophys. Res. Lett.*, 32, L22809,
7 doi:10.1029/2005GL024322, 2005.

8 Rickards, A. M. J., Miles, R. E. H., Davies, J. F., Marshall, F. H. and Reid, J. P.: Measurements of the sensitivity
9 of aerosol hygroscopicity and the κ parameter to the O/C ratio, *J. Phys. Chem. A*, 117, 14120–14131,
10 doi:10.1021/jp407991n, 2013.

11 Rissler, J., Vestin, A., Swietlicki, E., Fisch, G., Zhou, J., Artaxo, P. and Andreae, M. O.: Size distribution and
12 hygroscopic properties of aerosol particles from dry-season biomass burning in Amazonia, *Atmos. Chem. Phys.*,
13 6, 471–491, 2006.

14 Santarpia, J. L., R. Gasparini, R. Li, and D. R. Collins: Diurnal variations in the hygroscopic growth cycles of
15 ambient aerosol populations, *J. Geophys. Res.*, 110, D03206, doi:10.1029/2004JD005279, 2005.

16 Schwarz, J. P., Perring, A. E., Markovic, M. Z., Gao, R. S., Ohata, S., Langridge, J., Law, D., McLaughlin, R.
17 and Fahey, D. W.: Technique and theoretical approach for quantifying the hygroscopicity of black-carbon-
18 containing aerosol using a single particle soot photometer *J. Aerosol Sci.*, 81., 110–126,
19 doi:10.1016/j.jaerosci.2014.11.009, 2015.

20 Sihto, S. L., Mikkilä, J., Vanhanen, J., Ehn, M., Liao, L., Lehtipalo, K., Aalto, P. P., Duplissy, J., Petäjä, T.,
21 Kerminen, V. M., Boy, M. and Kulmala, M.: Seasonal variation of CCN concentrations and aerosol activation
22 properties in boreal forest, *Atmos. Chem. Phys.*, 11, 13269–13285, doi:10.5194/acp-11-13269-2011, 2011.

23 Stokes, R. H. and Robinson, R. A.: Interactions in aqueous nonelectrolyte solutions. I. Solute-solvent equilibria,
24 *J. Phys. Chem.*, 70, 2126–2131, doi:10.1021/j100879a010, 1966.

25 Suda, S. R., Petters, M. D., Matsunaga, A., Sullivan, R. C., Ziemann, P. J. and Kreidenweis, S. M.:
26 Hygroscopicity frequency distributions of secondary organic aerosols, *J. Geophys. Res.*, 117, D04207,
27 doi:10.1029/2011JD016823, 2012.

28 Tang, I. N.: Chemical and size effects of hygroscopic aerosols on light scattering coefficients, *J. Geophys. Res.*,
29 101, 19245–19250, 1996.

30 Toon, O. B., Pollack, J. B., and Khare, B. N., The optical constants of several atmospheric aerosol species:
31 Ammonium sulfate, aluminum oxide, and sodium chloride, *J. Geophys. Res.*, 81, 5733-
32 5748, doi:10.1029/JC081i033p05733, 1976.

33 [van Donkelaar A., Martin, R. V., Brauer, M., and Boys B. L.: Use of satellite observations for long-term](#)
34 [exposure assessment of global concentrations of fine particulate matter, *Environ. Health Perspect.* 123, 135–143,](#)
35 [doi:10.1289/ehp.1408646, 2015.](#)

29

Brock et al. Aerosol Hygroscopicity in the Southeastern [U.S.-US](#)

Formatted: Position: Horizontal: Left,
Relative to: Column, Vertical: In line,
Relative to: Margin, Wrap Around

1 Varma, R. M., Ball, S. M., Brauers, T., Dorn, H. P., Heitmann, U., Jones, R. L., Platt, U., Pöhler, D., Ruth, A.
2 A., Shillings, A. J. L., Thieser, J., Wahner, A. and Venables, D. S.: Light extinction by secondary organic
3 aerosol: an intercomparison of three broadband cavity spectrometers, *Atmos. Meas. Tech.*, 6, 3115–3130,
4 doi:10.5194/amt-6-3115-2013, 2013.

5 [Voss, K., Welton, E., Quinn, P., Frouin, R., Miller, M. and Reynolds, R.: Aerosol optical depth measurements](#)
6 [during the Aerosols99 experiment, *J. Geophys. Res.*, 106, 20821–20831, doi:10.1029/2000JD900783, 2001.](#)

7 Wagner, N. L., Brock, C. A., Angevine, W. M., Beyersdorf, A., Campuzano-Jost, P., Day, D. A., de Gouw, J. A.,
8 Diskin, G. S., Gordon, T. D., Graus, M. G., Huey, G., Jimenez, J. L., Lack, D. A., Liao, J., Liu, X., Markovic, M.
9 Z., Middlebrook, A. M., Mikoviny, T., Peischl, J., Perring, A. E., Richardson, M. S., Ryerson, T. B., Schwarz, J.
10 P., Warneke, C., Welti, A., Wisthaler, A., Ziemba, L. D. and Murphy, D. M.: In situ vertical profiles of aerosol
11 extinction, mass, and composition over the southeast United States during SENEX and SEAC⁴RS: observations
12 of a modest aerosol enhancement aloft, *Atmos. Chem. Phys.*, 15, 7085-7102, doi:10.5194/acp-15-7085-2015,
13 2015.

14 Warren, S. G., Hahn, C. J., London, J., Chervin, R. M., and Jenne, R. L.: Global Distribution of Total Cloud
15 Cover and Cloud Type Amounts over Land., NCAR Tech. Note TN-273_STR, 1–232,
16 <http://www.atmos.washington.edu/CloudMap/Publications/index.html>, 1986.

17 Washenfelder, R. A., Attwood, A. R., Brock, C. A., Guo, H., Xu, L., Weber, R. J., Ng, N. L., Allen, H. M.,
18 Ayres, B. R., Baumann, K., Cohen, R. C., Draper, D. C., Duffey, K. C., Edgerton, E., Fry, J. L., Hu, W. W.,
19 Jimenez, J. L., Palm, B. B., Romer, P., Stone, E. A., Wooldridge, P. J. and Brown, S. S.: Biomass burning
20 dominates brown carbon absorption in the rural southeastern United States, *Geophys. Res. Lett.*, 42,
21 10.1002/2014GL062444, 2015.

22 Wex, H., Petters, M. D. and Carrico, C. M.: Towards closing the gap between hygroscopic growth and activation
23 for secondary organic aerosol: Part I-Evidence from measurements, *Atmos. Chem. Phys.*, 9, 3987-3997, 2009.

24 Wright, H. L.: Atmospheric opacity: a study of visibility observations in the British Isles, *Q. J. R. Meteor. Soc.*,
25 65, 411-442, 1939.

26 Xu, L., Guo, H., Boyd, C. M., Klein, M., Bougiatioti, A., Cerully, K. M., Hite, J. R., Isaacman-VanWertz, G.,
27 Kreisberg, N. M., Knote, C., Olson, K., Koss, A., Goldstein, A. H., Hering, S. V., de Gouw, J., Baumann, K.,
28 Lee, S.-H., Nenes, A., Weber, R. J., and Ng, N. L.: Effects of anthropogenic emissions on aerosol formation
29 from isoprene and monoterpenes in the southeastern United States, *Proc. Nat. Acad. Sci.*, 112, 37-42, 2015a.

30 Xu, L., Suresh, S., Guo, H., Weber, R. J. and Ng, N. L.: Aerosol characterization over the southeastern United
31 States using high-resolution aerosol mass spectrometry: spatial and seasonal variation of aerosol composition
32 and sources with a focus on organic nitrates, *Atmos. Chem. Phys.*, 15, 7307–7336, doi:10.5194/acp-15-7307-
33 2015, 2015b.

34 Zaveri, R. A.: A new method for multicomponent activity coefficients of electrolytes in aqueous atmospheric
35 aerosols, *J. Geophys. Res.*, 110, D02201, doi:10.1029/2004JD004681, 2005.

30

Brock et al. Aerosol Hygroscopicity in the Southeastern [U.S.](#)

Formatted: Widow/Orphan control,
Adjust space between Latin and Asian
text, Adjust space between Asian text
and numbers, Tab stops: Not at 0.99
cm + 1.98 cm + 2.96 cm + 3.95 cm +
4.94 cm + 5.93 cm + 6.91 cm +
7.9 cm + 8.89 cm + 9.88 cm +
10.86 cm + 11.85 cm

Formatted: Widow/Orphan control,
Adjust space between Latin and Asian
text, Adjust space between Asian text
and numbers, Tab stops: Not at 0.99
cm + 1.98 cm + 2.96 cm + 3.95 cm +
4.94 cm + 5.93 cm + 6.91 cm +
7.9 cm + 8.89 cm + 9.88 cm +
10.86 cm + 11.85 cm

Formatted: Position: Horizontal: Left,
Relative to: Column, Vertical: In line,
Relative to: Margin, Wrap Around

1 Zhang, Q., Jimenez, J. L., Canagaratna, M. R., Allan, J. D., Coe, H., Ulbrich, I., Alfarra, M. R., Takami, A.,
2 Middlebrook, A. M., Sun, Y. L., Dzepina, K., Dunlea, E., Docherty, K., DeCarlo, P. F., Salcedo, D., Onasch, T.,
3 Jayne, J. T., Miyoshi, T., Shimojo, A., Hatakeyama, S., Takegawa, N., Kondo, Y., Schneider, J., Drewnick, F.,
4 Borrmann, S., Weimer, S., Demerjian, K., Williams, P., Bower, K., Bahreini, R., Cottrell, L., Griffin, R. J.,
5 Rautiainen, J., Sun, J. Y., Zhang, Y. M. and Worsnop, D. R.: Ubiquity and dominance of oxygenated species in
6 organic aerosols in anthropogenically-influenced Northern Hemisphere midlatitudes, *Geophys. Res. Lett.*, 34,
7 L13801, doi:10.1029/2007GL029979, 2007.

8 [Zieger, P., Weingartner, E., Henzing, J., Moerman, M., de Leeuw, G., Mikkilä, J., Ehn, M., Petäjä, T., Clémer,
9 K., van Roozendaal, M., Yilmaz, S., Frieß, U., Irie, H., Wagner, T., Shaiganfar, R., Beirle, S., Apituley, A.,
10 Wilson, K., and Baltensperger, U.: Comparison of ambient aerosol extinction coefficients obtained from in-situ,
11 MAX-DOAS and LIDAR measurements at Cabauw, *Atmos. Chem. Phys.*, 11, 2603–2624, doi:10.5194/acp-11-
12 2603-2011, 2011.](#)

13 [Zieger, P., Kienast-Sjögren, E., Starace, M., von Bismarck, J., Bukowiecki, N., Baltensperger, U., Wienhold, F.
14 G., Peter, T., Ruhtz, T., Collaud Coen, M., Vuilleumier, L., Maier, O., Emili, E., Popp, C. and Weingartner, E.:
15 Spatial variation of aerosol optical properties around the high-alpine site Jungfraujoch \(3580m a.s.l.\), *Atmos.
16 Chem. Phys.*, 12, 7231–7249, doi:10.5194/acp-12-7231-2012, 2012.](#)

17 [Zieger, P., Fierz-Schmidhauser, R., Weingartner, E. and Baltensperger, U.: Effects of relative humidity on
18 aerosol light scattering: results from different European sites, *Atmos. Chem. Phys.*, 13, 10609–10631,
19 doi:10.5194/acp-13-10609-2013, 2013.](#)

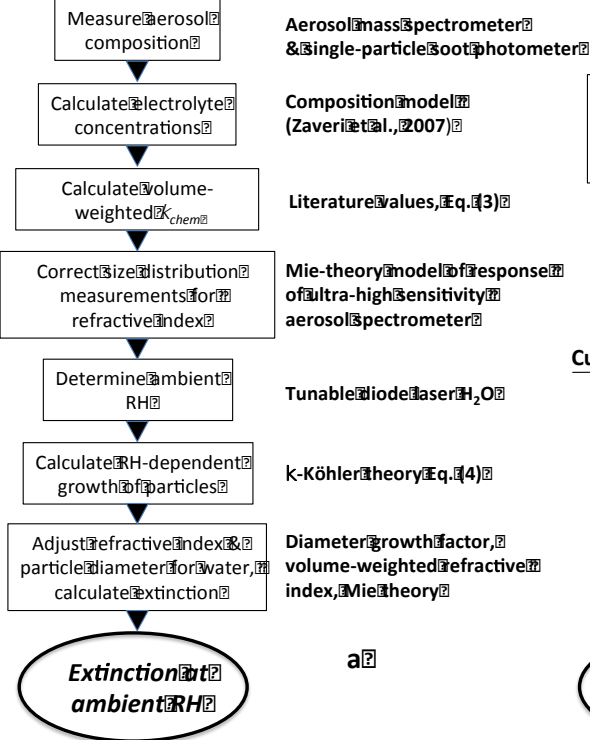
20 [Zieger, P., Fierz-Schmidhauser, R., Poulain, L., Müller, T., Birmili, W., Spindler, G., Wiedensohler, A.,
21 Baltensperger, U. and Weingartner, E.: Influence of water uptake on the aerosol particle lightscattering
22 coefficients of the Central European aerosol, *Tellus B*, 66, 22716, doi:10.3402/tellusb.v66.22716, 2014.](#)

23 [Zieger, P., Aalto, P. P., Aaltonen, V., Äijälä, M., Backman, J., Hong, J., Komppula, M., Krejci, R., Laborde, M.,
24 Lampilahti, J., de Leeuw, G., Pfüller, A., Rosati, B., Tesche, M., Tunved, P., Väänänen, R. and Petäjä, T.: Low
25 hygroscopic scattering enhancement of boreal aerosol and the implications for a columnar optical closure study,
26 *Atmos. Chem. Phys.*, 15, 7247–7267, doi:10.5194/acp-15-7247-2015, 2015.](#)

27 [Ziemba, L. D., Hudgins, C. H., Obland, M. D., Rogers, R. R., Scarino, A. J., Winstead, E. L., Anderson, B. E.,
28 Thornhill, K. L., Ferrare, R., Barrick, J., Beyersdorf, A. J., Chen, G., Crumeyrolle, S., Hair, J. and Hostetler, C.
29 A.: Airborne observations of aerosol extinction by in-situ and remote-sensing techniques: Evaluation of particle
30 hygroscopicity, *Geophys Res Lett*, doi:10.1029/2012GL054428, 2012.](#)

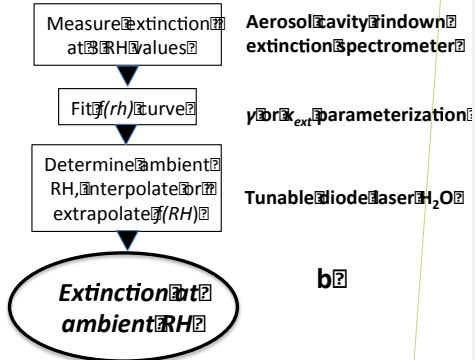
31
32

Explicit Köhler method



Two approaches to calculate extinction at ambient RH from in situ measurements

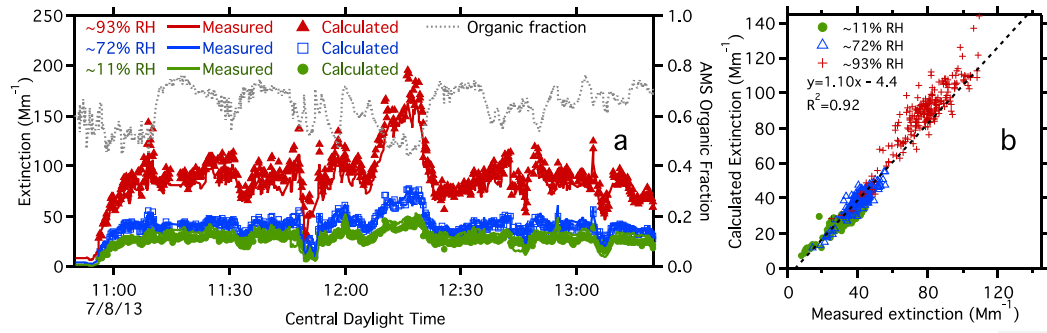
Curve-fitting ($y = \text{brk}_{ext}$) method



Formatted: Font: Italic

- 1
- 2
- 3
- 4
- 5

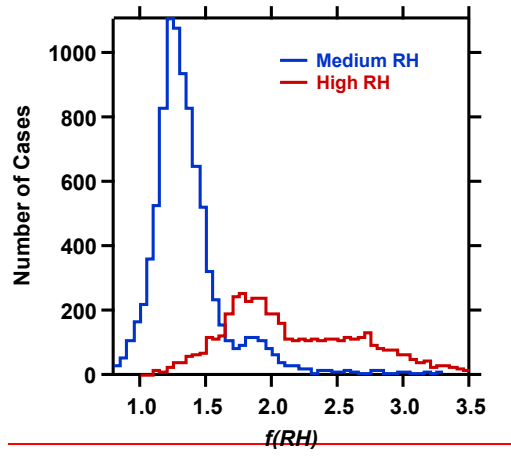
Figure 1. Schematics showing the process of calculating ambient extinction from a) measurements of composition, size distribution, and ambient RH and b) measurements of ambient RH and of extinction at three instrumental RH values.



1
2
3
4
5
6
7

Figure 2. a) Measured and calculated extinction at three RH values (left axis) and the organic fraction of fine aerosol mass (right axis) measured near local noon on 8 July 2013. b) Calculated vs. measured ambient extinction for all three RH values from (a) over the time period from 11:10 and 11:45 local time. Dashed line is a two-sided linear least-squares regression.

1



2

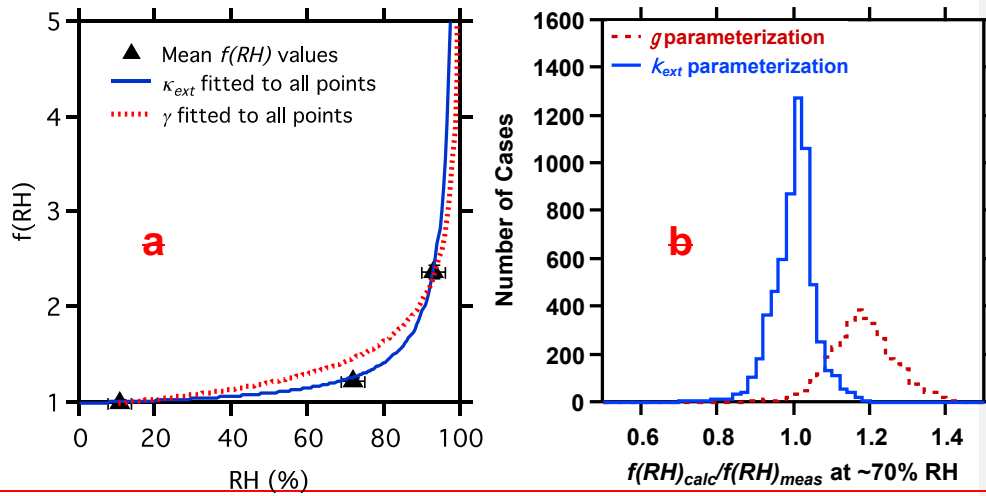
3

Figure 3. Histograms of values of $f(RH)$ measured at medium RH ($70 \pm 3\%$) and at high RH ($90 \pm 3\%$) for the SENEX and SEAC4RS data selected for this study.

5

6

1



2

3

4 **Figure 4.** Mean values of $f(RH)$ determined from measurements between 11:10 and 11:45 local time on 8
5 July 2013 from Fig. 2 (symbols), and curves from the γ power law parameterization (dashed line, Eq. (1))
6 and the κ_{ext} parameterization (solid line, Eq. (6)) fitted to the three data points. Error bars show the standard
7 deviation of the mean values. b) Ratio of calculated to measured $f(RH)$ at ~70% RH for the γ and κ_{ext}
8 parameterizations for all analyzed data.

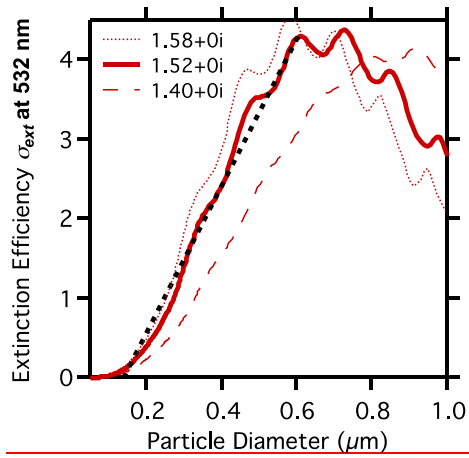
9

10

11

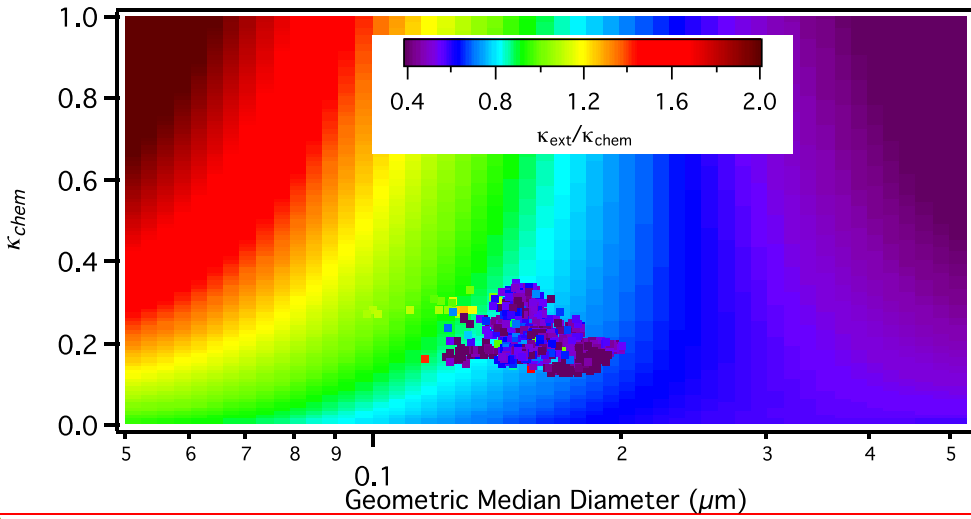
12

13



1
2
3
4
5
6

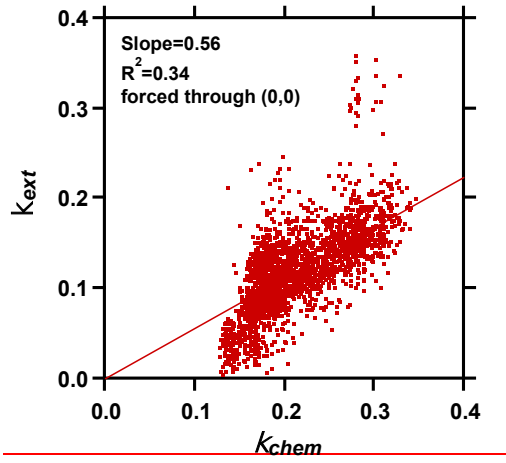
Figure 5. Calculated extinction efficiency for a particle with a refractive index of $1.52+0i$ (solid line) and linear least squares fit for particle diameters between $0.1\mu\text{m}$ and $0.6\mu\text{m}$ (dashed line). The extinction efficiency averaged across the size range of hygroscopic growth of a typical accumulation mode aerosol is approximately linear. Extinction efficiency curves for $1.58+0i$ and $1.40+0i$ are also shown.



Formatted: Font: Italic

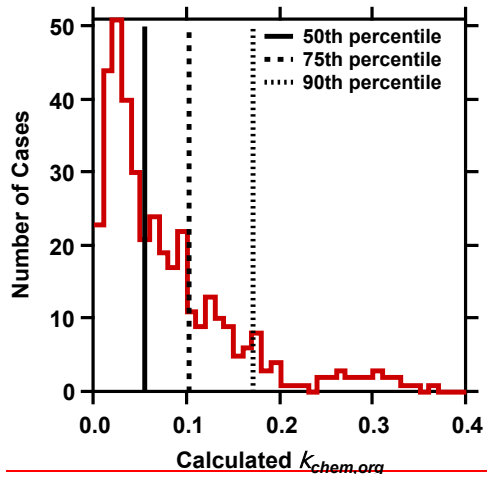
1
2
3
4
5
6
7

Figure 6. Ratio of optically determined κ_{ext} to chemically determined κ_{chem} as a function of particle geometric median diameter and κ_{chem} . Values of κ_{ext} were calculated for a lognormal particle size distribution with a geometric standard deviation of 1.5 and a geometric median diameter given by the abscissa. Points are instantaneous values of $\kappa_{ext}/\kappa_{chem}$ determined from the in-situ $f(RH)$ and composition measurements.



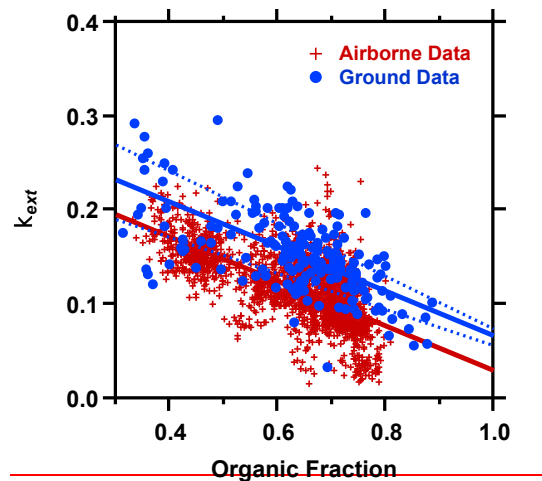
1
2
3
4

Figure 7. Values of κ_{ext} determined from fitting Eq. (6) to the $f(RH)$ data plotted as a function of κ_{chem} calculated from aerosol composition measurements using κ Köhler theory (Eq. (3)).



1

2 ~~Figure 8. Histogram of results from a Monte Carlo analysis showing values of the organic $\kappa_{chem,org}$ that, given~~
 3 ~~the observed inorganic composition and size distribution, are consistent within experimental uncertainty~~
 4 ~~with the measured $f(RH)$. Vertical lines indicate the 50th, 75th, and 90th percentile values of the histogram.~~



1
2
3
4
5

Figure 9. Comparison of κ_{ext} as function of the fraction of sub- $0.7\mu\text{m}$ non refractory OA for the data analyzed in this paper (crosses) and similar measurements at the SOAS ground site in Centreville, Alabama, U.S. (Washenfelder et al., 2014) between the hours of 11:00 and 17:00 local time (circles). Dashed lines show regressions to the Centreville data if κ_{ext} is calculated using RH values that vary by the uncertainty of $\pm 3\%$ RH.

Formatted: English (U.S.)

Formatted: Position: Horizontal: Left, Relative to: Column, Vertical: In line, Relative to: Margin, Wrap Around

Figure Captions

Figure 1. Schematics showing the process of calculating ambient extinction from a) measurements of composition, size distribution, and ambient RH and b) measurements of ambient RH and of extinction at three instrument RH values.

Figure 2. Map of the southeastern U.S. showing state borders and tracks of the flights during SENEX and SEAC4RS. Triangles show the locations of the 37 vertical profiles that are used in this analysis; 25 of these had valid $f(\text{RH})$ measurements. The location of the groundsite in Centreville, Alabama is indicated. The inset shows the eastern portion of the U.S.; the dashed box indicates the sample region.

Figure 3. A vertical profile measured from 18:29 to 18:35 UTC on 22 June 2013 over east-central Alabama. a) Extinction measured in the dry, medium, and high RH channels of the CRDS, extinction calculated using the fitting method described in Section 3.4, and extinction at ambient RH calculated using this method. The dashed horizontal lines show the boundaries between the well-mixed and transition layers and between the transition layer and free troposphere, as defined by Wagner et al. (2015). b) Measured RH values within the dry, medium, and high RH channels of the CRDS, and ambient RH. c) $f(\text{RH})$ measured at the medium and high RH conditions, and calculated from fitted values as in (a). Circles show the $f(\text{RH})$ values from fitting Eq. 6 to the $f(\text{RH})$ data. Triangles show the fraction of sub- $0.7\ \mu\text{m}$ aerosol mass measured by the AMS that is inorganic (top axis).

Figure 4. Composite vertical profiles of a) dry extinction, b) $f(\text{RH})$ at $\sim 70\%$ RH, and c) $f(\text{RH})$ at $\sim 90\%$ RH. Shaded areas represent the interdecile and interquartile ranges. The dashed horizontal lines in (a) show the boundary between the well-mixed and transition layers and between the transition layer and free troposphere, as defined by Wagner et al. (2015). The circles and dashed lines in (b) and (c) show the mean $f(\text{RH})$ values determined by fitting the κ_{ext} and γ parameterizations, respectively, to the raw data before altitude binning and averaging. The triangles in (c) show the fraction of sub- $0.7\ \mu\text{m}$ aerosol mass measured by the AMS that is inorganic (top axis); error bars show the interquartile range.

Figure 5. a) Calculated $f(\text{RH})$ compared with observed $f(\text{RH})$ at $\sim 70\%$ RH using the methodology in Fig. 1a for all analyzed data. Lines are 2-sided least squares (orthogonal distance regression) fits to the data. The dashed line is calculated assuming the line passes through (1,1). b) As in (a), but for $\sim 90\%$ RH. Organic hygroscopicity ($\kappa_{\text{chem,OA}}$) is assumed to be 0.05.

Figure 6. Histogram of results from a Monte Carlo analysis showing values of the organic κ_{chem} that, given the observed inorganic composition and size distribution, are consistent within experimental uncertainty with the measured $f(\text{RH})$. Vertical lines indicate the 50th, 75th, and 90th percentile values of the histogram.

Figure 7. a) Mean values of $f(\text{RH})$ determined profile data in the well-mixed and transition layers (below 2000 m altitude) on 22 June 2013 over central Alabama from Fig. 3c (symbols), and curves from the γ power-law parameterization (dashed line, Eq. (1)) and the κ_{ext} parameterization (solid line, Eq. (6)) fitted to the three data points. The green hashed line shows a fit to the γ parameterization assuming

Formatted: Heading 1

Formatted: Left: 3.17 cm, Right: 3.02 cm, Top: 2.54 cm, Bottom: 2.54 cm, Width: 20.99 cm, Height: 29.66 cm, Header distance from edge: 1.27 cm, Footer distance from edge: 1.27 cm

Formatted: Font: Not Italic

Formatted: Font: Not Italic

Formatted: Font: Not Italic

Formatted: Font: Not Italic

Formatted: Position: Horizontal: Left, Relative to: Column, Vertical: In line, Relative to: Margin, Wrap Around

RH₀=35% (see Sect. 3.4). Error bars show the propagated measurement uncertainties and measurement standard deviation. b) Histograms of values of f(RH) measured at medium RH (70+/-3%) and at high RH (86-94%) for all of the data selected for this study. c) Ratio of calculated to measured f(RH) at ~70% RH for the γ and κ_{ext} parameterizations for all of the data selected for this study.

Figure 8. Comparison of κ_{ext} as function of the fraction of sub-0.7 μm non-refractory OA for the data analyzed in this paper (crosses) and similar measurements at the SOAS ground site in Centreville, Alabama, U.S. (Washenfeller et al., 2014) between the hours of 11:00 and 17:00 local time (circles).

Figure A1. Calculated extinction efficiency for a particle with a refractive index of 1.52+0i (solid line) and linear least-squares fit for $0.1 < D_p < 0.6$ (dashed line). The extinction efficiency averaged across the size range of hygroscopic growth of a typical accumulation mode aerosol is approximately linear. Extinction efficiency curves for 1.58+0i and 1.40+0i are also shown.

Figure A2. Ratio of optically determined κ_{ext} to chemically determined κ_{chem} as a function of particle geometric median diameter and κ_{chem} . Values of κ_{ext} were calculated for a lognormal particle size distribution with a geometric standard deviation of 1.5 and a geometric median diameter given by the abscissa. Points are instantaneous values of $\kappa_{\text{ext}}/\kappa_{\text{chem}}$ determined from the in situ f(RH) and composition measurements.

Figure A3. Values of κ_{ext} determined from fitting Eq. (6) to the f(RH) data plotted as a function of κ_{chem} calculated from aerosol composition measurements using κ -Köhler theory (Eq. 3).

Figure A4. Values of f(RH) from rooftop measurements of ambient and dry extinction made at Boulder, Colorado, US, from 2015/03/05 to 2015/06/04. Curves are two-sided least-squares fits to the data using the κ_{ext} and \square parameterizations. Data are selected for periods when κ_{chem} determined from measurements made with the C-TOF-AMS were < 0.4 .

Formatted: English (U.S.)

Formatted: Position: Horizontal: Left, Relative to: Column, Vertical: In line, Relative to: Margin, Wrap Around